SUBMISSION TO TUNNELLING AND UNDERGROUND SPACE TECHNOLOGY

TUST_2019_113R1

FIRST SUBMISSION: 27 January 2019

REVISED VERSION: 15 November 2019

TITLE:

Evaporation-induced soil water flux to design suction drain for low-carbon ground stabilisation: experimental investigation and modelling

AUTHORS:

Michela Martini*

Alessandro Tarantino **

POSITION AND AFFILIATION:

* PhD, UNOPS, Health, Safety, Social and Environmental Management, København, Denmark, formerly Department of Civil and Environmental Engineering, University of Strathclyde, Glasgow, UK

** Professor, Department of Civil and Environmental Engineering, University of Strathclyde

CONTACT ADDRESS:

Alessandro Tarantino
Department of Civil and Environmental Engineering
University of Strathclyde
James Weir Building - Level 5
75 Montrose Street - Glasgow G1 1XJ, Scotland, UK
E-mail: alessandro.tarantino@strath.ac.uk

KEYWORDS

Water evaporation; Airflow; Suction drain; Ground-stability.

EVAPORATION-INDUCED SOIL WATER FLUX TO DESIGN SUCTION DRAIN FOR LOW-CARBON GROUND STABILISATION: EXPERIMENTAL INVESTIGATION AND MODELLING

Abstract

The suction drain is a novel concept for low-carbon temporary ground stabilisation in clayey soils alternative to jet grouting and ground freezing. Boreholes are drilled into the ground and air is injected to the borehole end through a delivery pipe. The air flowing through the gap between the pipe and the borehole surface backward towards the borehole entry removes water by evaporation and, hence, increases the undrained shear strength of the soil surrounding the drain. There are no studies that allow quantifying soil water evaporation generated by tangential airflow for the case of 'wind tunnel' only a few centimetres high over an evaporating surface a few meters long. This paper first presents an experimental investigation on water evaporation induced by air flow. A 3m long wet surface was subjected to tangential air flow into a 40mm gap. Tests were carried out by considering different air velocities and inlet air relative humidity. A model was then formulated to quantify the water evaporation rate for any length of the wet surface. The model parameters were calibrated against one experimental dataset and the model was then validated against an independent dataset. Finally, an empirical equation is proposed to estimate model parameters without the need of carrying out experimental tests. This is based on the vapour transfer coefficient established empirically for evaporation from open water (external air flow), which was found to remain valid for confined evaporation (internal air flow). The paper therefore provides a tool to estimate airflow-induced evaporation to successfully design the suction drains.

1 Introduction

Stability of tunnels and excavations in soft clays is major challenge in underground construction due to the relatively low shear strength of the clay. In saturated clays, shear

strength is controlled by the pore-water pressure under drained conditions (via the effective stress) and the soil water content under undrained conditions (Wood, 1991). Shear strength can then be increased by lowering the pore-water pressure or the soil water content depending on whether long-term (drained) or short-term (undrained) conditions are considered respectively. Approaches to deplete pore-water pressure and water content includes prefabricated drains (Sakleshpur et al. 2018) or vacuum consolidation drains (Griffin & O'Kelly, 2014). Water is drained by imposing a pressure in the drain lower than the pore-water in the surrounding soil, which is atmospheric (nil gauge pressure) in the prefabricated drain or nominally equal to -100 kPa gauge pressure in the vacuum consolidation drains.

The suction drain is an innovative concept for temporary stabilisation of tunnels and excavations in clays. The soil is exposed to the air flowing tangentially to the surface of a drilled borehole. When a saturated clay is exposed to the air flow, evaporation takes place at the clay surface. Water is initially removed without displacement of the gas–liquid–solid junction of the outer menisci. The meniscus curvature then increases and pore-water pressure in the clay drops to values lower than atmospheric pressure. In clays under saturated conditions, pore-water pressure reduces to values even lower than the absolute zero pressure, i.e. pore-water is being held in tension (Tarantino 2010). As a result, pore-water is driven towards the drain under hydraulic gradients much higher than prefabricated or vacuum consolidation drains, making the suction drain potentially much more efficient.

This concept was developed in Martini et al. (2019) for short-term tunnel face stabilisation and is based on the principle that undrained cohesion is enhanced by depleting soil water content. The concept of the suction drain is shown in Figure 1. A borehole is drilled into the ground and centralised air delivery tube is positioned into the borehole. This is used to inject compressed air to the end of the borehole. The air flows from the end of the borehole to its entry through the gap between the centralised air delivery tube and the inner surface of the borehole. The air that flows tangentially to the inner surface of the drilled borehole exposes the soil to

evaporation. Water flows towards the borehole therefore reducing the water content of the surrounding soil and increasing the soil shear strength. The suction drain is designed to be installed below the groundwater table. Drilling the borehole in the saturated zone will generate water flow towards the borehole, which would eventually fill up with water if there were no suction drain. However, if the evaporation rate at the borehole wall generated by the tangential airflow exceeds the natural influx towards the borehole, the borehole will remain dry and pore-water pressure surrounding the suction drain will be depleted from positive to negative values.

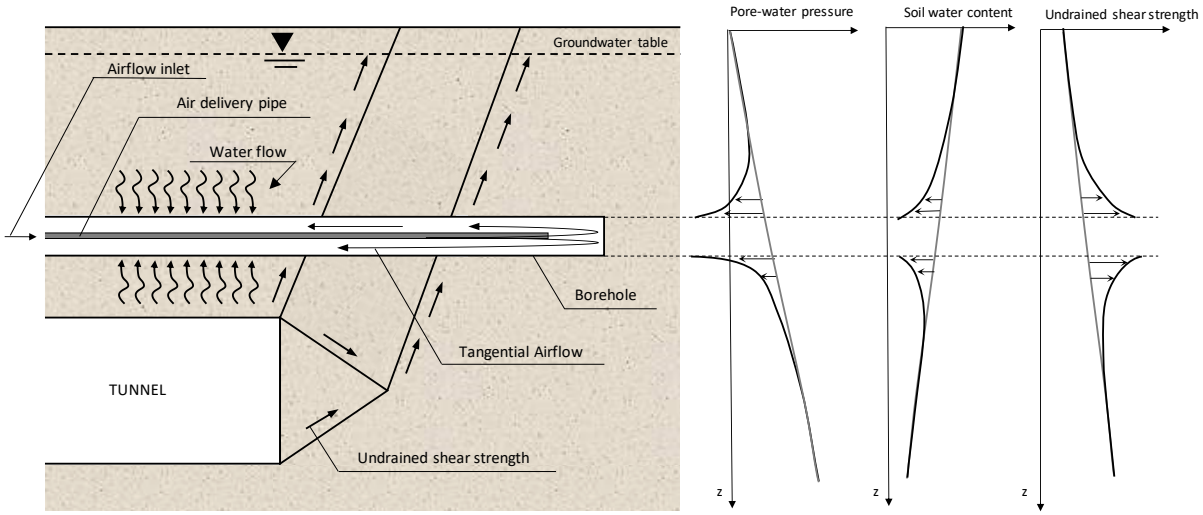

Figure 1: Concept of the suction drain (not to scale)

The key of this technique is therefore the water outflow generated by the air-flow, which needs to be quantified to design suction drains for ground stabilisation. Evaporation from a wet surface (free water or soil water) subjected to parallel air flow have been extensively investigated via climatic/evaporation chambers (Talev et al. 2008; Song et al. 2013, 2014; Davarzani et al. 2014; Lozada et al. 2016, 2018; Barghi 2018). However, these experiments have involved evaporating surface lengths of the same order of magnitude of the wind tunnel heights. This implies that the concentration boundary layer barely develops along the evaporating surface and convective water mass transfer occurs essentially under conditions of

'external flow'. The boundary layers develop freely without constraints imposed by adjacent surfaces and there exist a region of the flow outside the boundary layer in which velocity and concentration gradients are negligible (Incropera and deWitt, 2002). Similarly, theoretical and semi-empirical models available the literature to estimate the convection mass transfer coefficient as a function of air velocity also refer to conditions of 'external flow' from open surfaces (Penman, 1946; Chu et al., 2010; Lim et al., 2012; Brutsaert, 2013).

On the other hand, the air flow conditions in the suction drain are entirely different. The length of the evaporating surface is much longer than the height of the air gap and 'internal flow' conditions establish. The boundary layers developing at the bottom and top of the 'wind tunnel' tends to merge at the centreline, viscous effects extend over the entire cross section, and the velocity profile no longer changes with increasing distance from the entrance after an initial hydrodynamic entrance region (Incropera and deWitt, 2002).

Theoretical formulations for the convection mass transfer coefficients can be derived for internal flow in circular tubes only for the case where a water film covers uniformly the inner surface of the circular tube (Incropera and deWitt, 2002). Unfortunately, theoretical solutions are not readily available for the case of the suction drain configuration, where air flow occurs in a concentric tube annulus, with 'velocity' boundary layers developing at both inner and outer tube surfaces and 'concentration' boundary layers only developing at the outer tube surface. This calls for a specific experiment to be designed to i) investigate the mechanisms of evaporation occurring under confined air flow mimicking suction drain conditions and ii) model the convective mass transfer coefficient as a function of air velocity.

This paper first presents an apparatus designed to mimic the evaporation process occurring in the suction drain. The 'evaporation machine' allows the injection of airflow over a 3m-long evaporation water surface under confined airflow. The air is injected at different velocities and values of relative humidity. The total water mass loss (evaporation) and the air relative humidity along the evaporation surface are measured. The core of the experimental

investigation concerns tests on free water because it is not easy to create a soil sample 3m-long for each of the tests where a specific combination of air velocity and air relative humidity is investigated. However, there is evidence in the literature that evaporation from free water surface does not differ from evaporation from a wet soil surface (Garitte et al., 2013, Barghi 2018). A test on a shorter 'evaporation machine' 0.5m-long including a soil sample was planned to corroborate this assumption.

The experimental results aim to lead to an 'accessible' model to estimate airflow-induced evaporation for any length of the evaporation surface, i.e. different from the length investigated experimentally. This model would be the key to design the suction drain air flow characteristics in terms of air velocity and relative humidity.

2 Equipment

2.1 Long evaporation machine

A long evaporation machine was designed as illustrated in Figure 2. The device is composed of a 4m long upper wind tunnel above a 3m long container. The wind tunnel inlet is connected to the air injection system as described in the next section and the wind tunnel outlet is open to atmosphere.

The wind tunnel is designed to allow the air to flow tangentially over the evaporating surface of liquid or soil placed in the lower container. The wind tunnel is 40mm high and 30mm wide and the container is 100mm high and 30mm wide. The lid of the channel was removable to ease the filling or emptying of the lower container with water or soil. Once in place, the lid was sealed using silicon grease. The wind tunnel and the lower container were manufactured by assembling Perspex acrylic extruded sheets 8mm thick joined together using epoxy resin.

The inner dimensions of the wind tunnel were chosen to generate Reynolds numbers *Re* similar to the ones expected in the suction drain concentric tube annulus

$$Re = \frac{u \cdot D_h}{\nu} \tag{1}$$

where u is the air velocity, D_h is the hydraulic diameter, and ν is the kinematic viscosity ($\nu = 1.5 \cdot 10^{-05}$ m^2/s for dry air at 20°C). In turn, the hydraulic diameters for the wind tunnel and the suction drain concentric tube annulus respectively are given by

$$D_h = \frac{2ab}{a+b} \qquad (Wind\ tunnel)$$
$$D_h = D_{outer} - D_{inner} \qquad (Suction\ drain\ concentric\ annulus) \tag{2}$$

where a and b are the width and height of the wind tunnel respectively, and D_{outer} and D_{inner} are the diameters of the outer and inner tubes, i.e. the inner diameter of the borehole perforated casing and the outer diameter of the air delivery pipe respectively. The Reynolds numbers are compared in Table 1 and highlight that air flow associated with Reynolds numbers associated with the transition zone between laminar and turbulent regime (2300< Re<10000 according to Incropera and deWitt, 2002).

Table 1: Reynolds number in evaporation machine wind tunnel and the suction drain concentric tube annulus

		Air velocity, u (m/s)			
		1	2	3	4
Re	Suction drain concentric tube annulus (D_{inner}=0.04m, D_{outer}=0.09m)	3314	6628	9942	13256
	Wind tunnel (a=0.03m, b=0.04m)	2273	4545	6818	9090

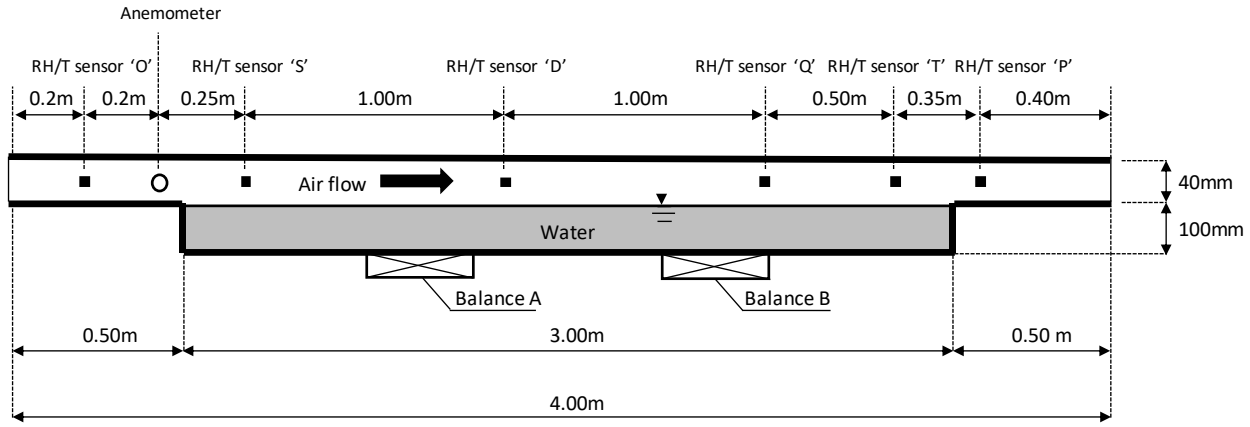

Figure 2: Layout of the long evaporation machine, RH=Relative Humidity, T=Temperature (not to scale)

Six sensors were placed in the wind tunnel to measure Relative Humidity (RH) and Temperature (T) (Sensirion Kit EK-H5 sensors SHT21) as shown in Figure 2. Holes were drilled into the lid to allow the cables of the Relative Humidity/Temperature (RH/T) sensors to pass through. These holes were sealed once the RH/T sensors were located mid-height and mid-width of the upper air channel with the RH/T sensing elements frontal to the airflow.

An anemometer (OMEGA FMA1006R-V2-S) was used to measure the airflow velocity. The anemometer was installed through the side wall of the channel at 0.4m from the inlet of the channel.

The evaporation machine was placed on two balances (ADAM CBK-32 and ADAM CBK-48) positioned 1.5m rightward from the inlet and 1.5m leftward from the outlet respectively (Figure 2). Balance readings were acquired at regular time lapse.

2.2 Short evaporation machine

A short evaporation machine was designed to assess the evaporation rate of water from a saturated soil sample exposed to tangential airflow. It is composed of 1.50m long wind tunnel and 0.5m long container (Figure 3). The dimensions of the cross section of both the upper wind tunnel and the bottom container are the same of those in the long evaporation machine.

Similarly, the lid of the upper wind tunnel was removable and sealed using silicon grease. The wind tunnel inlet was connected to the air injection system with the bypass for dry air as described in the next section. The wind tunnel outlet was open to atmosphere.

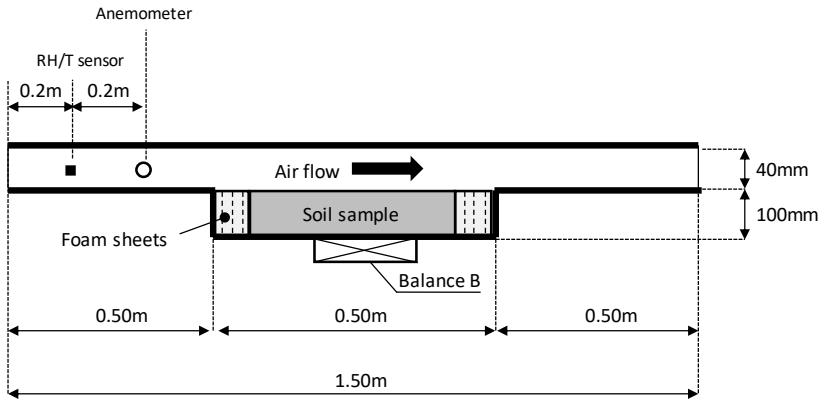

Figure 3: Layout of the short evaporation machine, RH=Relative Humidity, T=Temperature (not to scale)

The anemometer OMEGA FMA1006R-V2-S was used to measure the airflow velocity and it was installed through the side wall of the channel at 0.4m from the inlet of the channel. The RH/T device measuring velocity and temperature of the air was located normal to the airflow mid-height and mid-width of the upper air channel. The short evaporation machine was placed on one balance (ADAM PGW6002e) positioned at the centre of the bottom container (Figure 3).

2.3 Humid air injection system

An air injection system was developed to control the velocity and the relative humidity of the air entering the wind tunnel.

As shown in Figure 4, air was supplied to the humid air injection system from the compressed air system of the laboratory. Two air lines were derived from the ring main distribution system and each line was regulated by a laboratory tap. The two lines were connected in parallel via a T connection to ensure the delivery of the highest target air velocity. A pressure regulator was installed downstream the T connection to adjust the velocity of the airflow.

When the relative humidity of the airflow required to be increased prior to be injected into the evaporation machine, the airflow was forced to pass through the humidification chamber and the intermediate chamber before reaching the wind tunnel via the divergent duct.

The humidification chamber consists of 1L capacity graduated glass cylinder containing water and sealed on top with a rubber bung. Two holes were drilled through the rubber bung to allow the inlet tube and the outlet tube to pass through. The inlet tube could be positioned at different heights into the glass cylinder (by forcing it to slide through the rubber bung) whereas the outlet tube was fixed in place in the rubber bung.

The mixing of the dry air supplied by the compressed air system with the saturated vapour above the free water inside the cylinder allowed the airflow to increase its relative humidity. The desired relative humidity was achieved by i) adding a pre-determined volume of water inside the glass cylinder (depending on the target air velocity) and ii) adjusting the vertical position of the inlet pipe with respect to the water surface (at the beginning and during the test).

The glass cylinder was half-immersed into a water bath (10L) to mitigate the drop in temperature inside the glass cylinder due to evaporation. The volume of water inside the bath was not sufficient to maintain a constant temperature (as measured by laboratory glass thermometer immersed in the water bath). Water temperature in the bath was maintained constant by periodically replacing (cooling) water in the bath with water at relatively high temperature.

The flow from the glass cylinder was conducted to an intermediate chamber to separate water droplets from the humid air (droplets were captured by gravity at the bottom of the intermediate chamber).

A divergent duct 100mm long with a gradually lofted transition between the 16mm diameter air delivery tube and the 46x46mm rectangular cross-section of the evaporation machine was installed at the inlet of the evaporation machine to reduce the turbulence of the airflow due to the enlargement of the section. The taper angle of the duct was designed to 7° to reduce the effects

of boundary layer separation across the connection according to (Chandavari, V., & Palekar, 2014). The duct was designed and manufactured by utilising a 3D printer (Simpson, 2017).

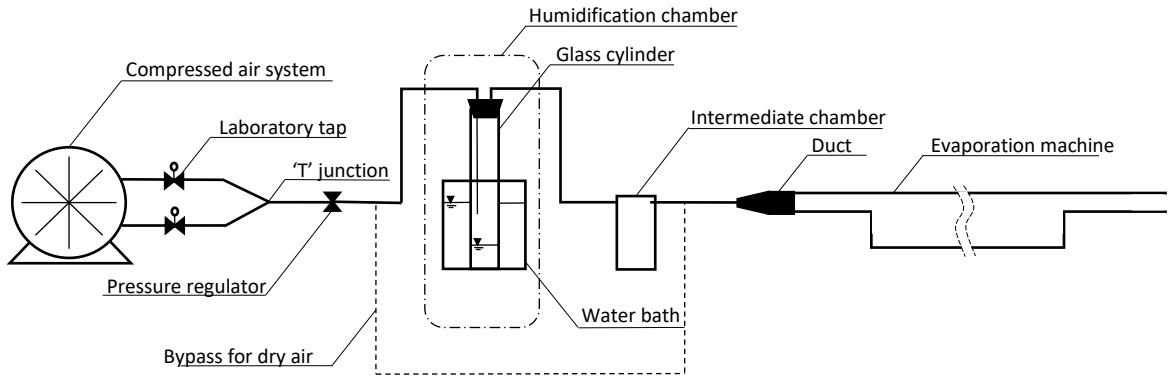

Figure 4: Layout of the air injection system (not to scale)

3 Experimental procedures

3.1 Long evaporation machine with water

The initial condition of each test consisted in establishing saturated vapour conditions in the wind tunnel. This was aimed at double-checking the readings from the Relative Humidity (RH) sensors before each test. To this end, the bottom container was filled with demineralised water until the water surface was lined up the base of the wind tunnel. The inlet and the outlet of the wind tunnel were sealed for approximately 10 h using Parafilm® and silicon grease and the relative humidity and the temperature were recorded continuously. It was then checked that the RH sensors were recording the same values within the accuracy expected in the range close to vapour saturation.

Two sets of tests are presented in the paper characterised by injected at a relative humidity of RH=0% and RH=30% respectively. The experimental procedure is first discussed for the test at RH=30%. Tests were run in a temperature-controlled laboratory (T=20±0.5°C). *Stage 1* - Before starting the air injection, the glass cylinder (Figure 4) was filled with a pre-determined volume of water and the position of the inner air delivery tube inside the cylinder was adjusted

to a pre-determined distance from the water level according to Table 2. These distances were determined by trial and error until a target relative humidity of RH=30% at the inlet of the upper air channel could be achieved. These distances were found to depend on the air velocities, which was ranged from 1 to 4 m/s. Airflow was not pointed directly to the water surface in the glass cylinder because this would have increased turbulence and caused significant amount of water droplets to be carried forward into the evaporation machine. The inner air delivery tube was therefore pointed towards the inner wall of the cylinder to break the air flow.

Table 2: Specifications of the test procedure in the long evaporation machine

Nominal air velocity (m/s)	Initial volume of water (ml)	Distance of the air delivery tube from the free water level (mm)	Target temperature of the water bath (°C)
1	300	114	25
2	180	160	28
3	150	171	35
4	100	190	40

Stage 2 - Laboratory taps were open and the pressure regulator was adjusted until the air velocity measured by anemometer attained the target air velocity with a maximum tolerance of ±0.05 m/s.

Stage 3 - All the Relative Humidity/Temperature (RH/T) sensors were switched on and the readings from the sensor at the inlet of the upper air channel (RH/T Sensor 'O' in Figure 2) was initially monitored. The position of the inner air delivery tube inside the cylinder was then fine adjusted until the RH was stable at 30%.

Stage 4 - The water bath was filled with water prepared at the pre-determined temperature specified in Table 2. Again these values were determined in preliminary tests by trial and error until a target temperature of 20°C at the inlet of the wind tunnel could be achieved (with a tolerance of ±2°C).

Stage 5 - The air velocity, the temperature, and the relative humidity at the inlet of the evaporation machine were monitored until stable values were reached. This phase typically took ~5-10 min. The RH sensors, the anemometer, and the balances were then logged as the test was assumed to start at this stage.

Stage 6 - During the test, the level of water inside the glass cylinder dropped as a result of evaporation. In turn, this caused the relative humidity at the inlet of the upper air channel to drop. When the relative humidity recorded by the sensor 'O' decreased from 30% to 25%, the inner air delivery tube was pushed downward into the cylinder until the relative humidity recorded by sensor 'O' increased to 35%. In this way, the relative humidity at the inlet was maintained at 30% with a tolerance of ±5%.

Stage 7 - During the test, the temperature of the water bath was monitored by using a glass laboratory thermometer immersed into the water bath. When the temperature of the water bath dropped by 2°C from the target temperature specified in Table 2, part of water in the bath was replaced with water at higher temperature until the temperature of the water bath regained the target value.

Stage 8 - The test was run for 2 h and this time was sufficient for all the sensors to attain stable values indicating that the system had reached a steady-state.

For the test involving injection of dry air in the wind tunnel (RH=0%), the humidification chamber and the intermediate chamber were by-passed as shown in Figure 4. In this case, the procedure only included Stages 2 and 5.

3.2 Short evaporation machine with soil

A core of soil between 3m and 4m from the ground level was sampled at the Bothkennar research Station in Falkirk by using the Terrier driller rig. After the sampling the core was stored in the plastic liner that was sealed at the two extremes to preserve the natural water content of the soil.

In the laboratory the initial water content of the soil was measured equal to w=50% and the initial soil suction was measured via the high-capacity tensiometer equal to s=35kPa. Under these conditions the soil sample was saturated. A rectangular undisturbed soil sample 118mm long, 17mm wide and 100mm high was trimmed from the core at the depth of 3.5m from the ground level.

The bottom and lateral surfaces of the cuboidal soil sample were covered by silica grease and Parafilm® to make them impermeable. The sample was placed at the centre of the bottom container as shown in Figure 3 and the empty space around the soil sample was filled with foam sheets to prevent eddies of air around the soil sample and to ensure that the air would flow tangentially over the top surface of the soil sample.

The small evaporation machine was connected to the air injection system with the bypass for dry air as explained in Section 2.3. The laboratory valves were opened until the velocity of the air, measured by the anemometer at the inlet of the wind tunnel was equal to v=4m/s. The airflow was maintained the time enough to ensure that the constant rate period of drying was achieved. The loss of mass of water from the top surface of the soil sample was recorded via the balance every 15min.

4 Experimental results

4.1 Long evaporation machine with water

4.1.1 Control of air velocity, relative humidity, and temperature

Figure 5 shows the air velocity measured via the anemometer at the inlet of the wind tunnel during each test. It can be observed that the air velocities were maintained constant to the nominal values specified in Table 2 throughout the duration of the tests with a standard deviation of the fluctuation that varies between ±0.02m/s (at lower air velocities) and ± 0.17m/s

(at higher air velocities). The control of the air velocity was considered satisfactory for the purpose of this study.

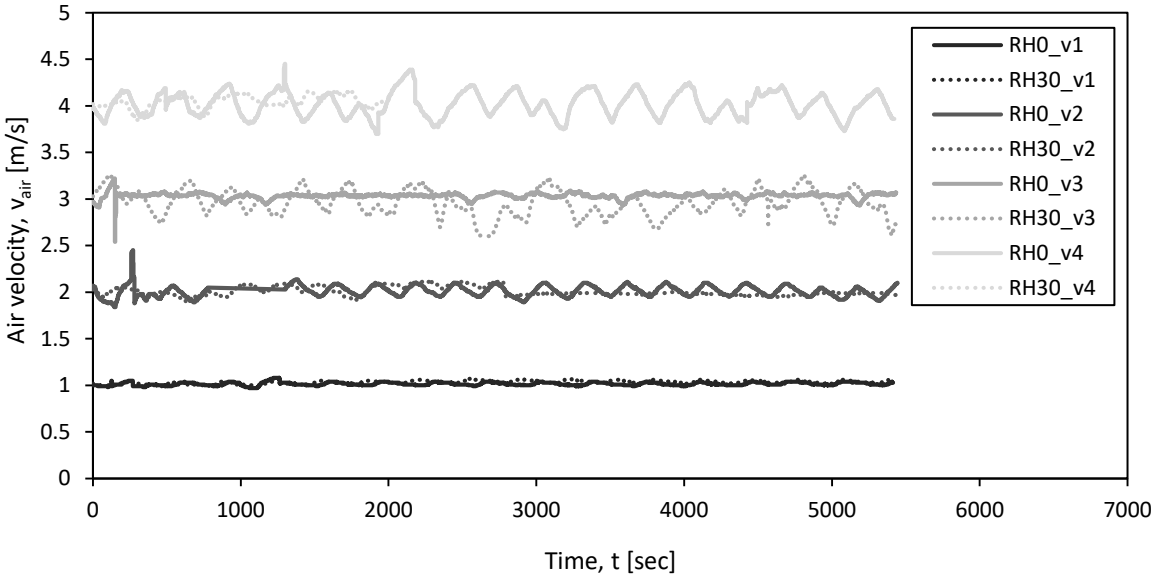

Figure 5: Air velocity recorded via the anemometer during the tests

Figure 6 shows the relative humidity *RH* of the airflow at the inlet of the wind tunnel measured by sensor 'O' during the tests with RH_{inlet}=30% and air velocities from v_{air}=1m/s to v_{air}=4m/s. The graph confirms the effectiveness of the humidification chamber to maintain the average relative humidity of the airflow at the inlet of the wind tunnel equal to RH_{inlet}=30% with a maximum standard deviation of the fluctuation equal to σ=±1.9%. The control of the relative humidity of the airflow at the inlet was then considered satisfactory.

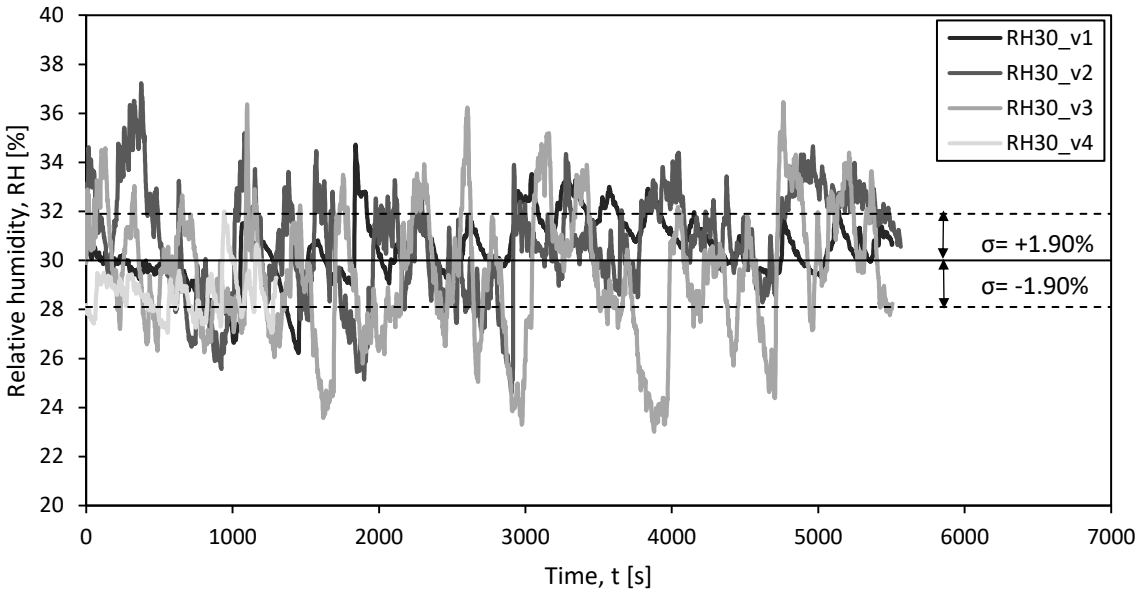

Figure 6: RH of the airflow at the inlet of the wind tunnel recorded by the sensor 'O' during the tests with RH_{inlet}=30%

Figure 7 shows the temperature of the airflow at the inlet of the wind tunnel measured by sensor 'O' during the tests with RH_{inlet}=30% and air velocities from v_{air}=1m/s to v_{air}=4m/s. As described in Section 3.1, the temperature of the airflow at the inlet of the wind tunnel was controlled by the temperature of the water bath in the humidification chamber. The graph shows the effectiveness of the method used to maintain the temperature constant to 20°C with a maximum standard deviation of the fluctuation equal to σ=±0.93% throughout the duration of each test. The control of the temperature of the airflow at the inlet was also considered satisfactory.

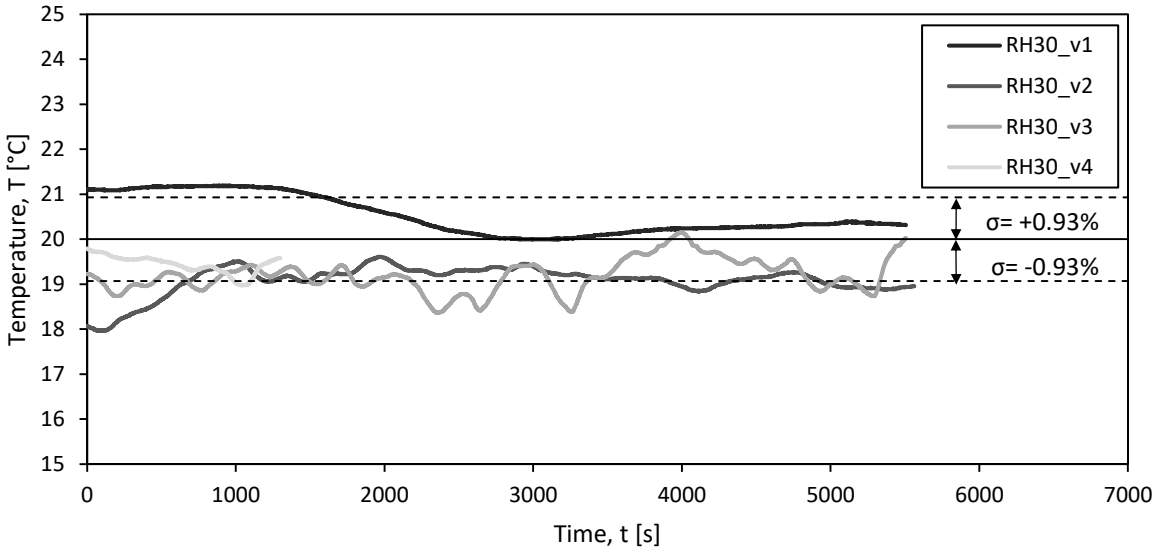

Figure 7: Temperature of the airflow at the inlet of the wind tunnel recorded by the sensor 'O' during the tests with RH_{inlet}=30%

4.1.2 Individual evaporation test

Figure 8 shows the typical relative humidity and temperature of the airflow recorded by the Relative Humidity/Temperature (*RH/T*) sensors over time along the wind tunnel during one of the tests with RH_{inlet}=30%. With reference to the relative humidity of the airflow it can be observed that the *RH* measured by each sensor is fairly stable throughout the duration of the test and that the responses of the sensors are in phase with each other. These findings suggest that the fluctuation recorded by each sensor is generated by the fluctuation of the relative humidity of the airflow imposed at the inlet. As one would expect, the relative humidity of the airflow progressively increases from the inlet to the outlet of the wind tunnel. The temperature of the airflow remains fairly constant at 20±1˚C over time along the wind tunnel. Interestingly, the first two sensors at the inlet of the wind tunnel (sensors 'O' and 'S') give the same values of relative humidity and temperature, which are slightly lower than the temperature of the airflow recorded by the other sensors. This suggests that both the temperature and the relative humidity of the first two sensors are controlled by the humidification chamber, whereas the relative humidity and the temperature measured by the other sensors is also influenced by the evaporating water in the bottom container.

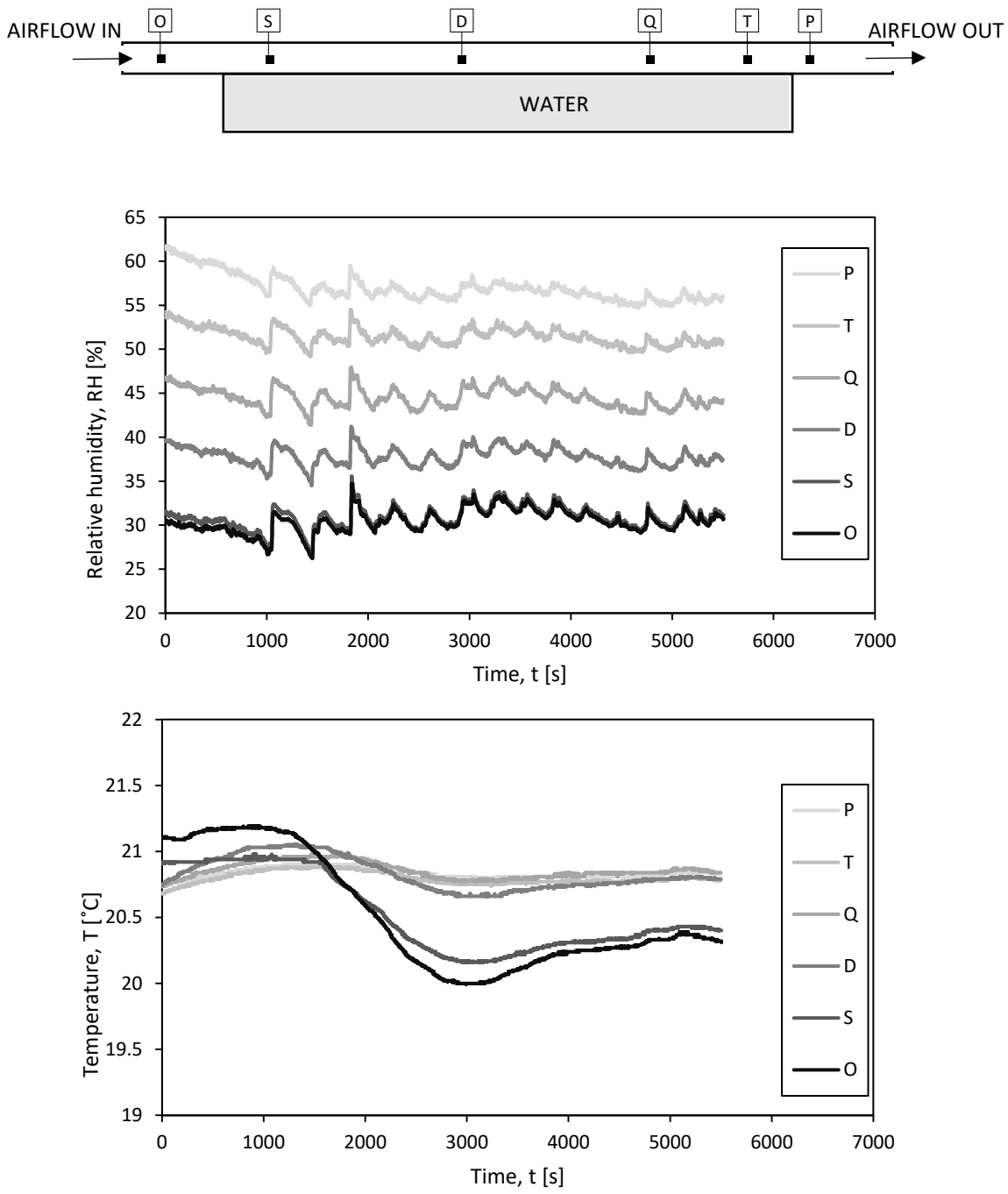

Figure 8: Typical reading of the relative humidity of the airflow (test with RH_{inlet}=30% and v_{air}=1m/s)

Figure 9 shows the criteria used to identify the steady state stage of each test for the computation of the relative humidity and the temperature of the airflow associated with and evaporation rate of water from the bottom container. Figure 9 refers to the test with RH_{inlet}=30% and v_{air}=1m/s; however similar results were obtained in the other tests. The first graph of Figure 9 shows the difference between the relative humidity measured by each sensor and the relative

humidity measured by sensor O plotted versus time. The second graph shows the data in terms of temperature processed in similar way. It can be observed that the difference of relative humidity and temperature between each sensor and sensor O decreases over time and reaches steady state after approximately 4000 seconds since the start of the test. The reading of the mass of the system versus time plotted in the third graph does not show a significant transition between the transient phase and the steady state phase in contrast with the relative humidity. This indicates that the fluctuation of the relative humidity and temperature of the airflow between the transient and the steady state does not affect significantly the evaporation rate.

All tests were interpreted by considering the average values of relative humidity, temperature, and evaporation rate under steady state conditions. i.e. over the period highlighted with a dotted window in Figure 9.

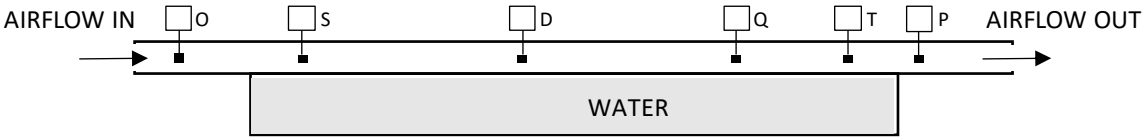
AIRFLOW IN
O
S
D
Q
T
P
AIRFLOW OUT
WATER

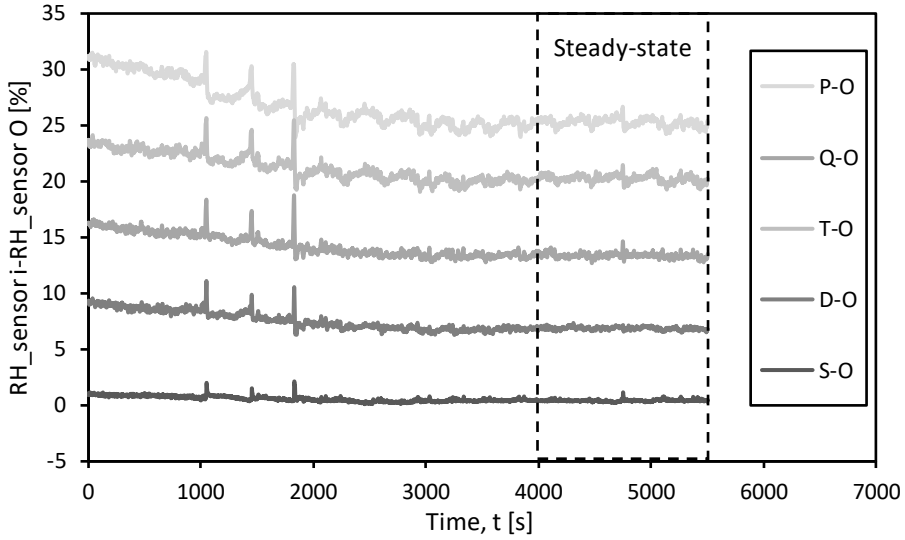
Steady-state
RH_sensor i-RH_sensor O [%]
Time, t [s]
P-O
Q-O
T-O
D-O
S-O

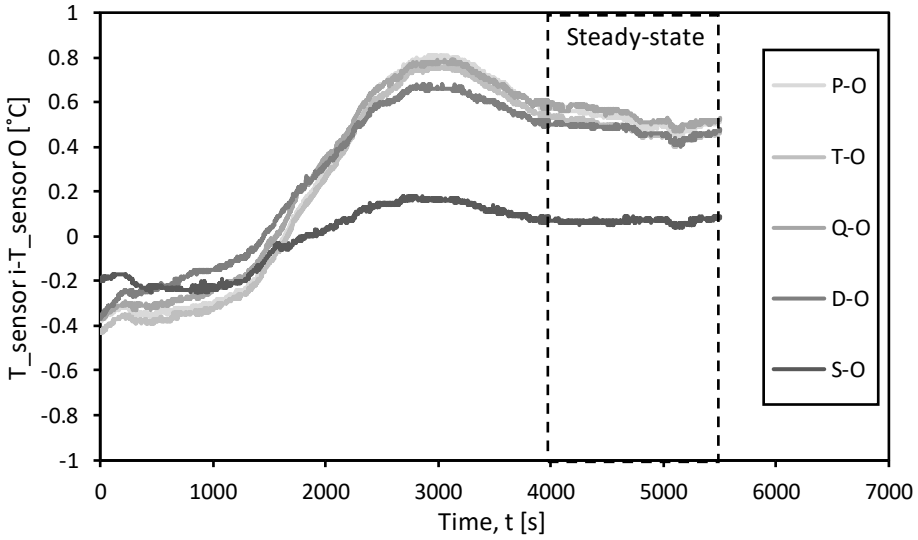
Steady-state
T_sensor i-T_sensor O [°C]
Time, t [s]
P-O
T-O
Q-O
D-O
S-O

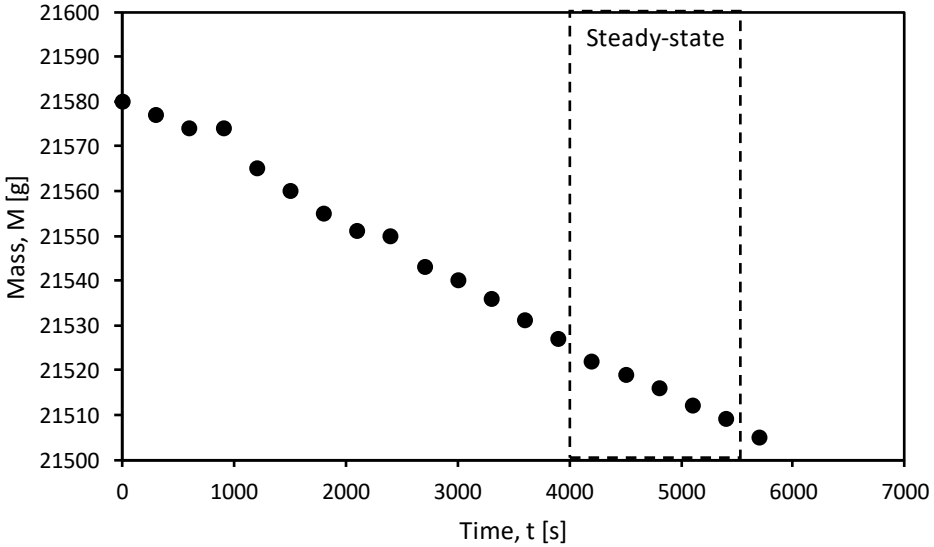
Steady-state
Mass, M [g]
Time, t [s]

Figure 9: Steady state phase of the test with RH_{inlet}=30% and v_{air}=1m/s

4.1.3 Evaporation tests at different relative humidity and air velocity

Figure 10 show the steady state values of relative humidity *RH* recorded along the wind tunnel in the tests at air velocity from v_{air}=1m/s to v_{air}=4m/s and relative humidity of the airflow at the inlet equal to RH_{inlet}=0% and RH_{inlet}=30% for Figure 10a and Figure 10b, respectively. The two dotted vertical lines represent the boundaries of the bottom water-filled container, sensor O provides the *RH* of the airflow at the inlet and sensor P provides the RH of the airflow at the outlet. Figure 10 shows that the relative humidity increases almost linearly with distance from the inlet. It can be observed that in each test the the relative humidity of the airflow measured by sensor 'S' is approximately equal to the relative humidity at the inlet recorded by sensor 'O'. A closer inspection to the relative humidity profile also shows that an accumulation of relative humidity of the air flow occurs at the outlet of the wind tunnel with air velocity v_{air}=1m/s. This boundary effect was probably due to some air stagnation for which the reason is not clear. It is also worth noticing that the relative humidity of the airflow at the outlet of the wind tunnel is greater when the airflow has a lower air velocity. This can be explained by the fact that high air velocity sweeps away evaporating water more efficiently.

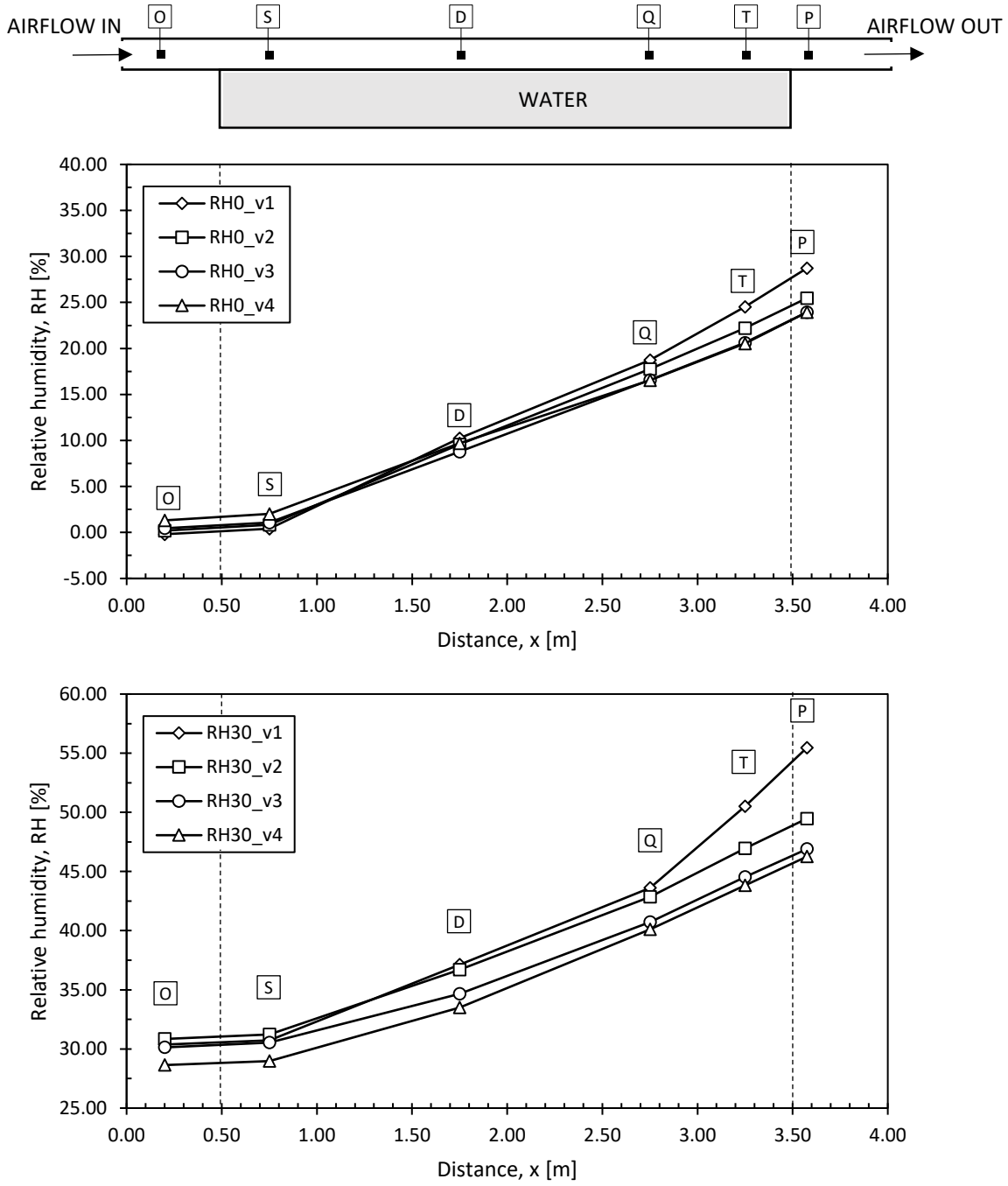

Figure 10: Relative humidity along the wind tunnel at different air velocity (and same relative humidity at the inlet RH_{inlet}).

Figure 11 compares the relative humidity profile at the same air velocity (v_{air}=1m/s) for the cases of relative humidity at the inlet equal to RH_{inlet}=0% and RH_{inlet}=30% respectively. It can be observed that the relative humidity of the airflow increases almost linearly along the wind tunnel in both tests. It is worth noticing that the increase of relative humidity between the inlet and the outlet in the test with RH_{inlet}= 0% is greater than the increase observed in the test with

RH_{inlet} =30%. This finding is consistent with the fact that the lower is the relative humidity of the airflow, the higher is the evaporation rate from the wet surface. With higher evaporation rate, the amount of water vapour carried by the tangential airflow above the wet surface increases and hence, the relative humidity of the airflow also increases.

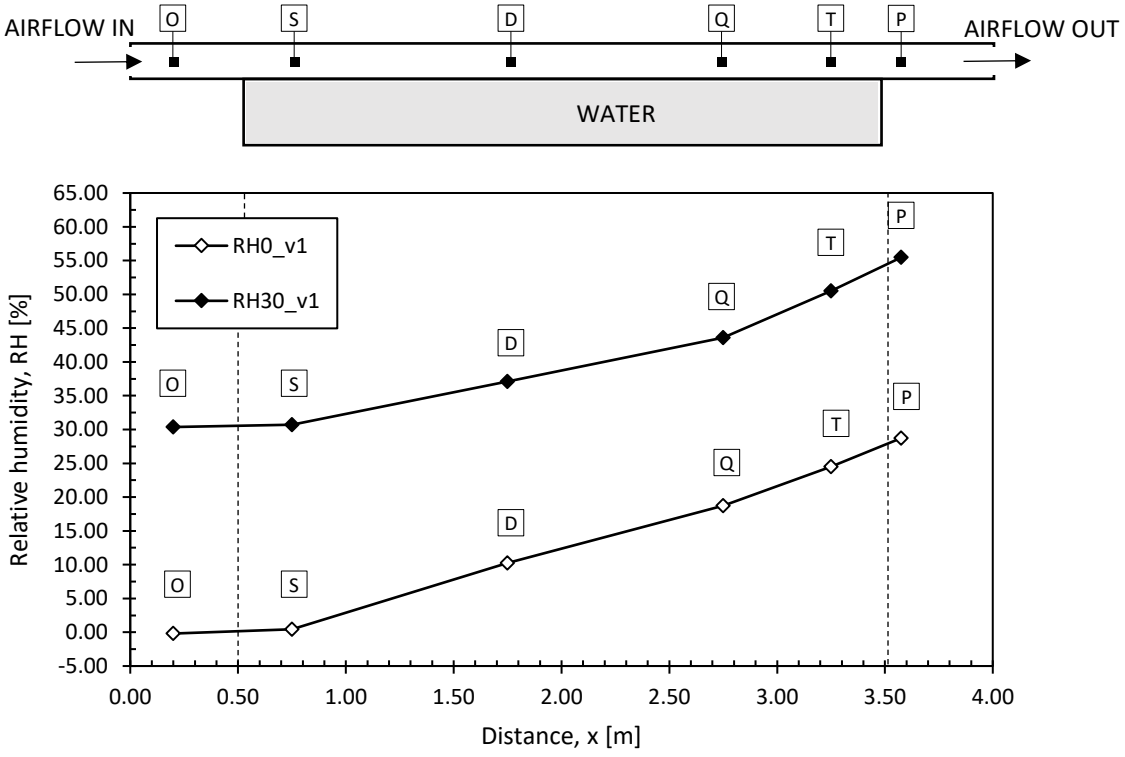

Figure 11: Relative humidity of the airflow along the wind tunnel-for different RH_{inlet} (and same air velocity v_{air}=1/ms)

Figure 12 shows the steady state temperature of the at air velocity from v_{air}=1m/s to v_{air}=4m/s and relative humidity equal to RH_{inlet}=0% and RH_{inlet} =30% in Figure 12a and Figure 12b respectively. It can be observed that the temperature of the airflow at the inlet could be maintained at 20±2˚C. In the tests with RH_{inlet} =0% the temperature of the airflow at the inlet was imposed by the compressed air system, whereas in the tests with RH_{inlet} =30% the temperature of the airflow was controlled by the temperature of the water bath in the humidification chamber. It is also possible to see that the temperature of the airflow remained fairly constant along the wind tunnel.

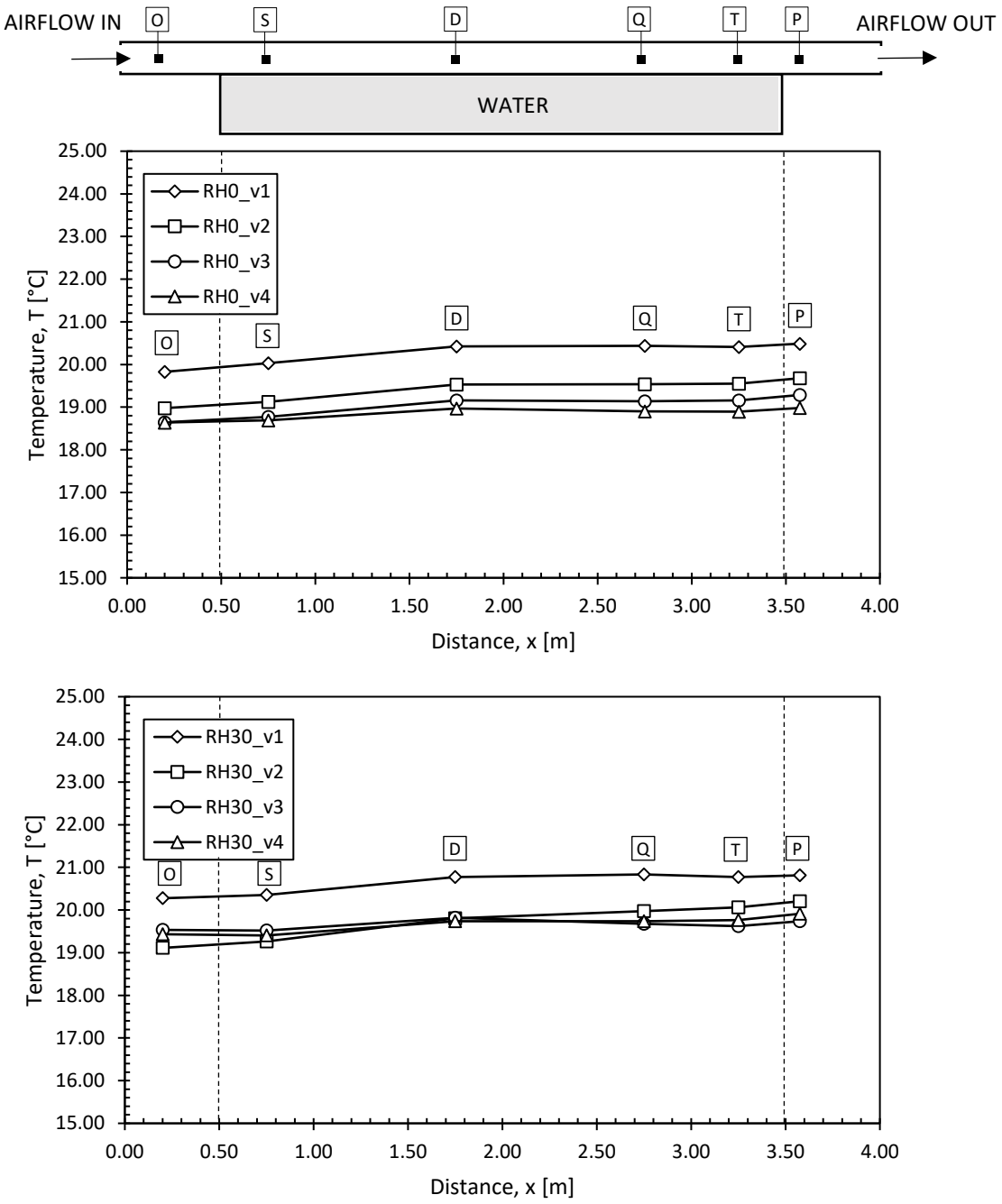

Figure 12: Temperature of the airflow measured at different air velocities and RH_{inlet} *=0% and* RH_{inlet} *=30%.*

A closer inspection of the temperature profile reveals that the temperature of the airflow slightly increases between the first two sensors (sensor 'O' and sensor 'D'), remains constant above the bottom container to slightly increases at the outlet (sensors 'T'and sensor 'P'). This suggests that the temperature of the airflow is controlled by the external boundary conditions

at the inlet and at the outlet of the wind tunnel whereas the temperature above the wet surface is slightly affected by the evaporation of the water from the bottom container.

The water flux q (volume of water per unit time and unit area) measured during the steady state of each test is plotted versus the air velocity v_{air} in Figure 13. As one would expect, the evaporation rate increases with air velocity and the evaporation rate is lower at higher relative humidity.

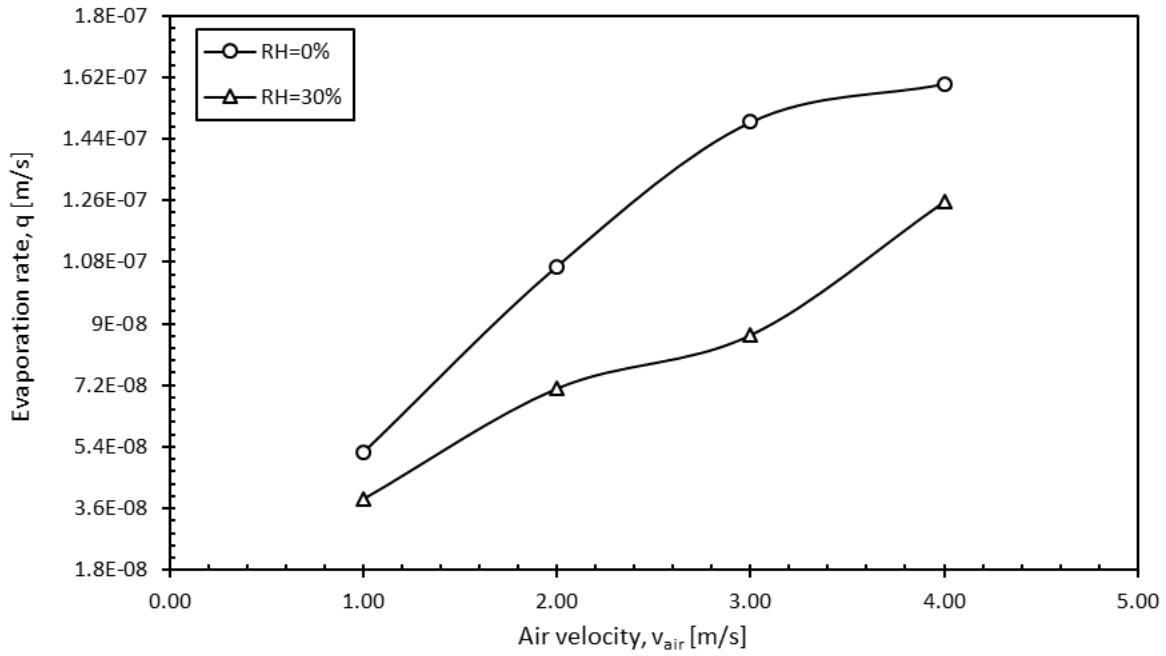

Figure 13: Experimental evaporation rate of water versus air velocity in the tests with RHinlet=0% and RHinlet=30%

The evaporation of water from a wet surface occurs due to the difference of relative humidity between the relative humidity at the wet surface (RH=100%) and the relative humidity in the mainstream flow above the wet surface. The higher is the relative humidity differential, the higher is the evaporation rate according to equation (9) shown later on in this paper (Section 5). On the other hand, higher airflow velocity maintains lower relative humidity in the mainstream flow and hence, higher relative humidity differential between the wet surface and the mainstream flow. As a result, the evaporation increases with air velocity. It is also worth

noticing that the two curves tend to converge at low air velocity, where the mechanism of evaporation by diffusion tends to dominate.

4.2 Short evaporation machine with soil

The loss of mass of water from the soil sample exposed to a tangential airflow with RH_{inlet}=0% and air velocity equals to v_{air}=4m/s in the short evaporation machine is plotted in Figure 14. It can be observed that the constant rate period of drying ends after approximately 3.5 hours from the start of the test. This stage can be associated with the saturated stage of the soil sample (Tarantino, A., et al., 2010).

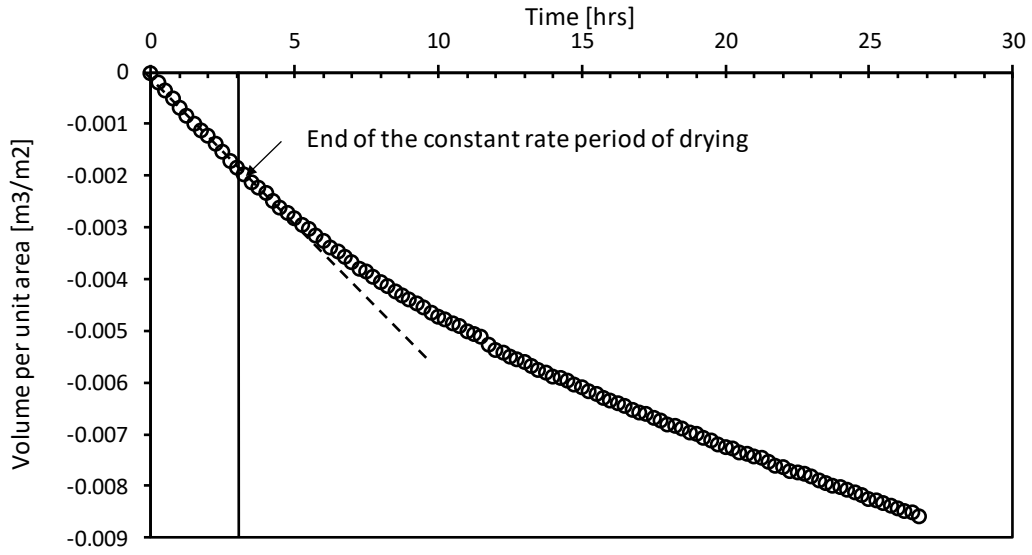

Figure 14: Loss of mass of water per unit area from the saturated soil sample over time

5 Water evaporation model

A model was developed to extend the results of the evaporation machine to suction drains that are longer than 3m and/or have airflow at the inlet with different relative humidity. The model was built by discretising the wind tunnel above the bottom water-filled container into elements 0.05m wide. For each element the following balance equation holds:

$$m_{in(i)} + m_{ev(i)} = m_{out(i)} = m_{in(i+1)} \quad (3)$$

where $m_{in(i)}$ is the mass of water vapour carried by the airflow at the inlet of the element (*i)*, $m_{ev(i)}$ is the mass of water that evaporates from the water surface at the bottom of the element (*i)*, $m_{out(i)}$ is the mass of water vapour carried by the airflow at the outlet of each element (*i),* and $m_{in(i+1)}$ is the mass of water vapour carried by the airflow at the inlet of the element (*i+1).*

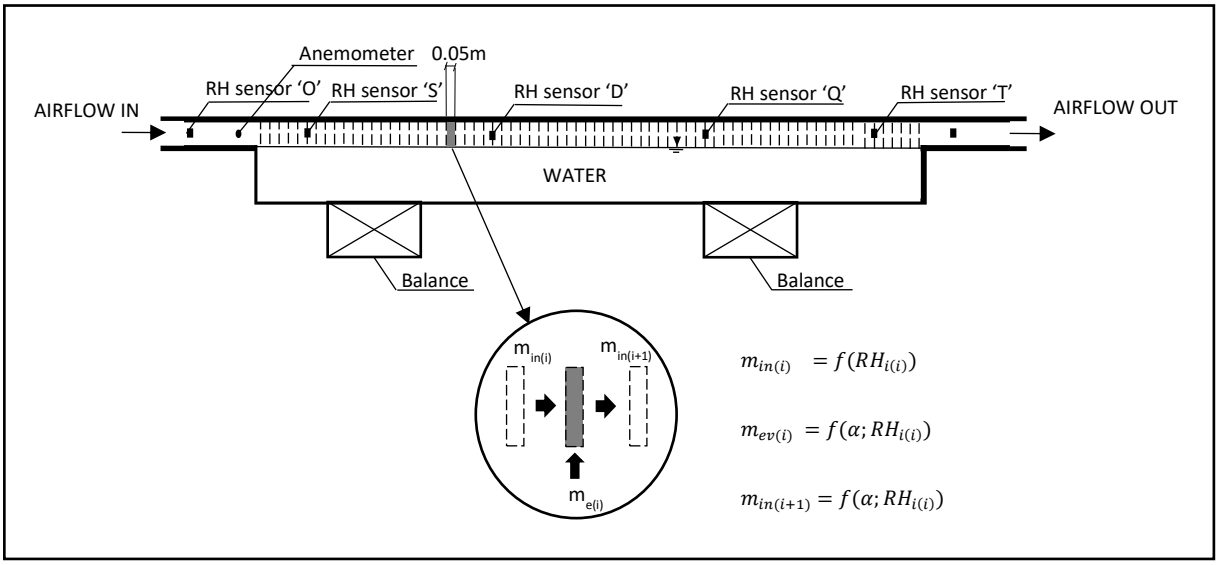

Figure 15: Graphical representation of the mass balance in the long evaporation machine for detecting the vapour transfer coefficient α

The mass of the water vapour at the inlet of each element $m_{in(i)}$ is expressed as:

$$m_{in(i)} = \rho_{v,i(i)} \cdot v_{air} \cdot \Delta t \cdot A_c \tag{4}$$

where $\rho_{v,i}$ is the density of the water vapour at the inlet of the element (*i)*, v_{air} is the velocity of the airflow measured via the anemometer at the inlet of the upper air channel, Δt is the time interval, and A_c is the cross sectional area of the upper air channel. In turn, the density of the water vapour at the inlet of the element $\rho_{v,in(i)}$ is a function of the relative humidity of the airflow at the inlet of the element (i), $RH_{in}(i)$. In turn, $RH_{in}(i)$ can be calculated as follows:

$$\rho_{v,in\,(i)} = \frac{p_{vo}\, RH_{in(i)}}{R_w T} \tag{5}$$

where p_{vo} is the equilibrium vapour pressure at saturation as a function of the temperature of the airflow, R_w is the gas constant of water vapour ($R_w = 461.50\, J\, K^{-1}\, kg^{-1}$) and T is the

absolute temperature. By combining equations (4) and (5), the mass of the water vapour at the inlet $m_{in(i)}$ can be derived from the relative humidity at the inlet $RH_{in}(i)$ as follows:

$$m_{in(i)} = \frac{p_{vo}\, RH_{in(i)}}{R_w T} \cdot v_{air} \cdot \Delta t \cdot A_c \tag{6}$$

Similarly, the mass of water vapour at the inlet of the element *(i+1)* can be derived from the relative humidity at the inlet $RH_{in(i+1)}$ as:

$$m_{in(i+1)} = \frac{p_{vo}\, RH_{in(i+1)}}{R_w T} \cdot v_{air} \cdot \Delta t \cdot A_c \tag{7}$$

The mass of water that evaporates from the water surface at the bottom of each element $m_{ev(i)}$ is described as follows:

$$m_{ev(i)} = q_{(i)} \cdot A_{ev} \cdot \Delta t \cdot \rho_w \tag{8}$$

where $q_{(i)}$ is the evaporation rate (water volume per unit area and unit time) in the element *(i)*, A_{ev} is the area of the water surface exposed to evaporation at the bottom of each element *(i)*, Δt is the time interval, and ρ_w is the density of liquid water. The evaporation rate of water per unit area and unit time $q_{(i)}$ under isothermal conditions is given by the Dalton equation:

$$q_{(i)} = \alpha(v_{air}) \cdot p_{vo} \cdot \left(1 - RH_{in(i)}\right) \tag{9}$$

where $\alpha(v_{air})$ is the vapour convective volume transfer coefficient, which is a function of the horizontal air velocity, p_{vo} is the equilibrium vapour pressure at saturation, $RH_{in(i)}$ is the relative humidity of the airflow at the inlet of the element *(i)*. By combining equations (8) and (9) the mass of the water that evaporates from the water surface at the bottom of each element *(i)* can be written as a function of α and $RH_{in(i)}$as follows:

$$m_{ev(i)} = \alpha(v_{air}) \cdot p_{vo} \cdot (1 - RH_{in(i)}) \cdot A_{ev} \cdot \Delta t \cdot \rho_w \tag{10}$$

It is worth mentioning that both the relative humidity and the velocity of the airflow are assumed to be uniform within the cross section of the wind tunnel in this model. The relative humidity of the airflow is assumed to be equal to RH=100% in contact with the wet surface

and to decrease sharply towards a constant value with height. Similarly, the air velocity is assumed to be v_{air} =0m/s in contact with the top and the bottom of the upper air channel and to increase sharply to a uniform value within the upper air channel as shown in Figure 16. The values of the uniform relative humidity and velocity of the air flow in the upper air channel are assumed to be equal to the values of relative humidity and air velocity measured experimentally via the relative humidity sensors and the anemometer at 20mm height from the wet surface.

The temperature profile (not shown in the figure) was assumed to be uniform across the upper air channel.

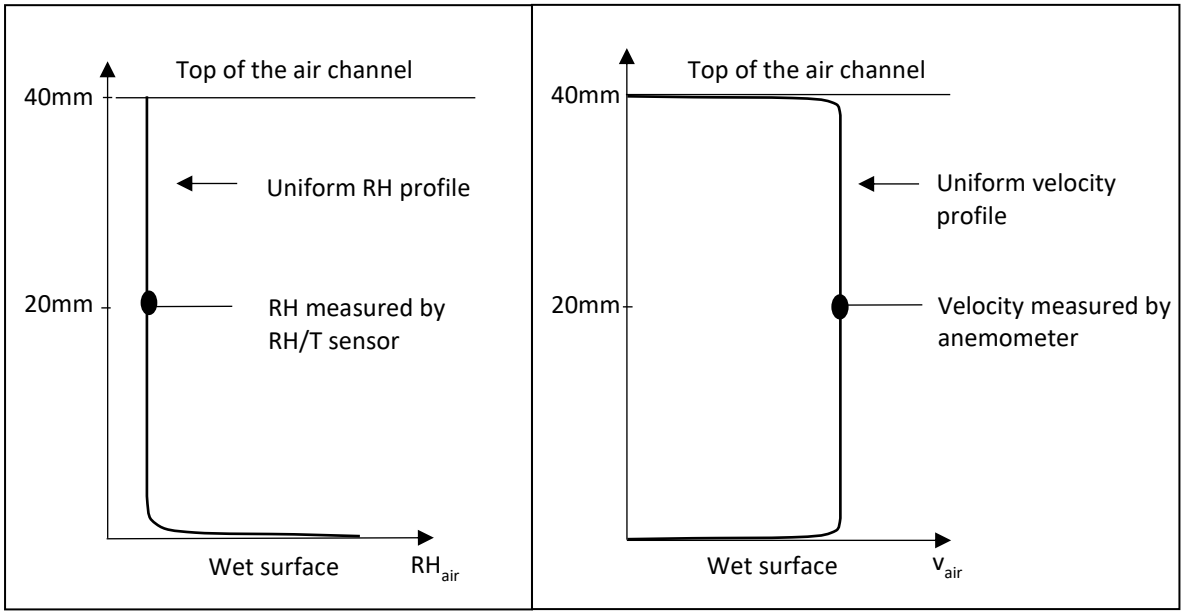

Figure 16: Uniform RH and velocity profile of the airflow in the upper air channel assumed in the model

5.1 Model calibration for water

The vapour transfer coefficient α model parameter was calibrated against the experimental results of the tests with the RH_{inlet}=0% and the air velocity varying from v_{air}=1m/s to v_{air}=4m/s. The relative humidity (*RH*) of the airflow at the inlet of the wind tunnel was assumed to be equal to the value measured by the sensor 'O' and was used as model input.

The vapour convective volume transfer coefficient α was calculated by imposing that:

$$q_{model} = \frac{\sum_1^n q_{(i),model} \cdot \Delta l_i}{\sum_1^n \Delta l_i} = q_{experimental} \quad (11)$$

where q_{model} is the overall evaporation rate returned by the model, $q_{(i),model}$ is the evaporation rate associated with the element *i*, Δl_i is the width of the element *i*, and $q_{experimental}$ is the overall evaporation rate measured via the balances in the tests with RH_{inlet}=0% and air velocity varying from v_{air}=1m/s to v_{air} =4m/s.

The evaporation rate (water volume per unit area and unit time) of each element *i*, $q_{(i),model}$, is a function of the vapour convective volume transfer coefficient α (the model parameter to be calibrated) and the relative humidity at the inlet of the element *i* $RH_{in(i)}$ derived from equation (9).

By combining equations (3), (6), (7), and (10) the relative humidity at the inlet of each element can be expressed as a function of the vapour convective volume transfer coefficient α. By imposing $RH_{in(1)} = RH_{sensor,0}$, the relative humidity RH profile can be derived by using a forward integration:

$$RH_{in(i+1)} = \left(RH_{in(i)} \cdot v_{air} \cdot A_c + \alpha \cdot p_{vo} \cdot \left(1 - RH_{in(i)}\right) \cdot A_{ev} \cdot \rho_w \cdot R_w \cdot T\right) \cdot \frac{\Delta t}{v_{air} \cdot A_c} \quad (12)$$

Once the $RH_{in(i)}$ is determined for each element, the water flow $q_{(i),model}$ for each element can be estimated via equation (9) and, hence, the overall evaporation rate, q_{model}. The vapour convective volume transfer coefficient α at given velocity v_{air} is then determined by imposing the equality given by equation (11) for each of the velocities varying from v_{air}=1m/s to v_{air} =4m/s. The parameters used for the model are listed in Table 3 and the values of the vapour convective volume transfer coefficient α derived from the calibration are shown *in Table 4*.

Table 3: Parameters of the model

T_0	$p_{v0}(T_0)$	R_w	Δt	A_c	A_{ev}	ρ_w
293.16 K	2333.44 Pa	461.9 J K^{-1} kg^{-1}	1 sec	0.0012 m^2	0.0015 m^2	998.2 kg/m^3

Table 4: Values of the vapour transfer coefficients derived from calibration

v_{air}	1 m/s	2 m/s	3 m/s	4 m/s
$\alpha(v_{air})$	2.43×10^{-11}	5.02×10^{-11}	6.94×10^{-11}	7.37×10^{-11}

5.2 Simulation of evaporation from water surface

Figure 17 shows the simulation of the evaporation rate, q_{model} simulated for airflow at RH_{inlet}=30% and air velocities varying from v_{air}=1m/s to v_{air} =4m/s compared with the evaporation rate $q_{experimental}$ obtained experimentally. The simulation of the test at RH_{inlet}=30% was based on the calibration of the vapour convective volume transfer coefficient α against an independent test (RH_{inlet} =0%) and discussed in Section 5.1. The model simulates satisfactorily the experimental results and it can therefore be considered an adequate tool to estimate the evaporation rate from the inner surface of the borehole exposed to a tangential airflow at a known air velocity.

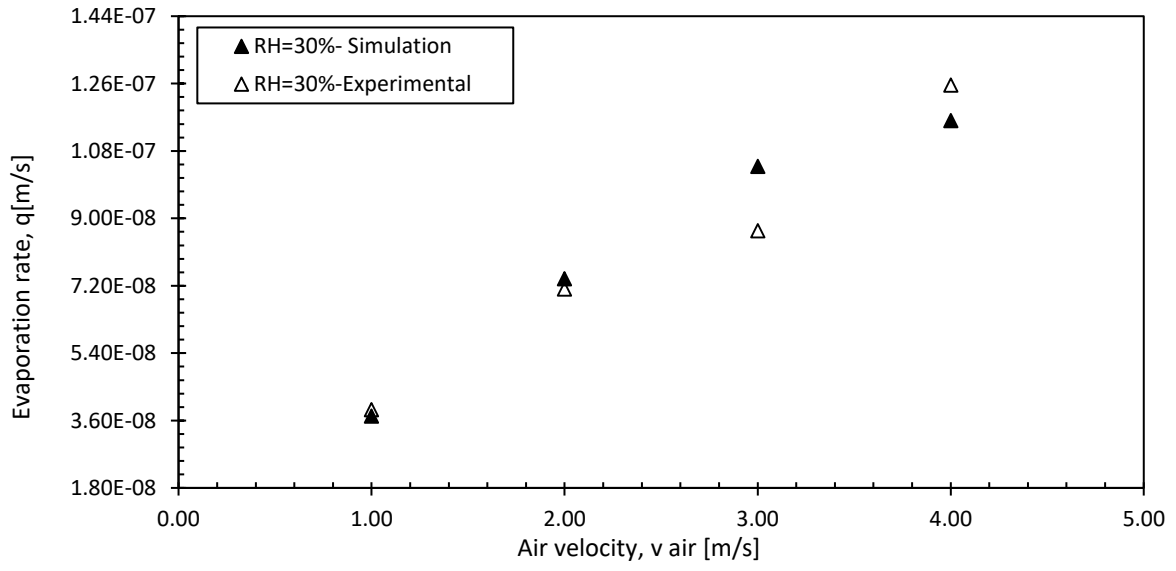

Figure 17: Comparison of the evaporation rate of water estimated via the model and obtained experimentally

5.3 Comparison between saturated soil and water surface

Figure 18 shows the comparison between the evaporation of water from the saturated soil surface in the short evaporation machine and the evaporation of water from the water surface in the long evaporation machine over time (both tests for an airflow having RH_{inlet}=0% and air velocity v_{air}=4m/s). The comparison is carried out in terms of the loss of water volume ΔV_{water} per unit area A normalised to the relative humidity differential ΔRH, i.e. the difference between the relative humidity at the evaporating surface (RH=100%) and the average relative humidity of the airflow in the wind tunnel above the evaporating surface ($RH_{average}$=0% for the soil sample in the short evaporation machine and $RH_{average}$=12% for the water surface in the long evaporation machine). The slope of the curves in Figure 18 actually represents the vapour convective volume transfer coefficient α.

The normalised water volume loss for soil and water compares favourably as shown in Figure 18. This suggests that the vapour convective volume transfer coefficient α derived from evaporation from water surface also holds for saturated soil sample. As a result, the outcomes of evaporation tests involving a wet surface water surface can be extrapolated to evaporation involving saturated soil surfaces.

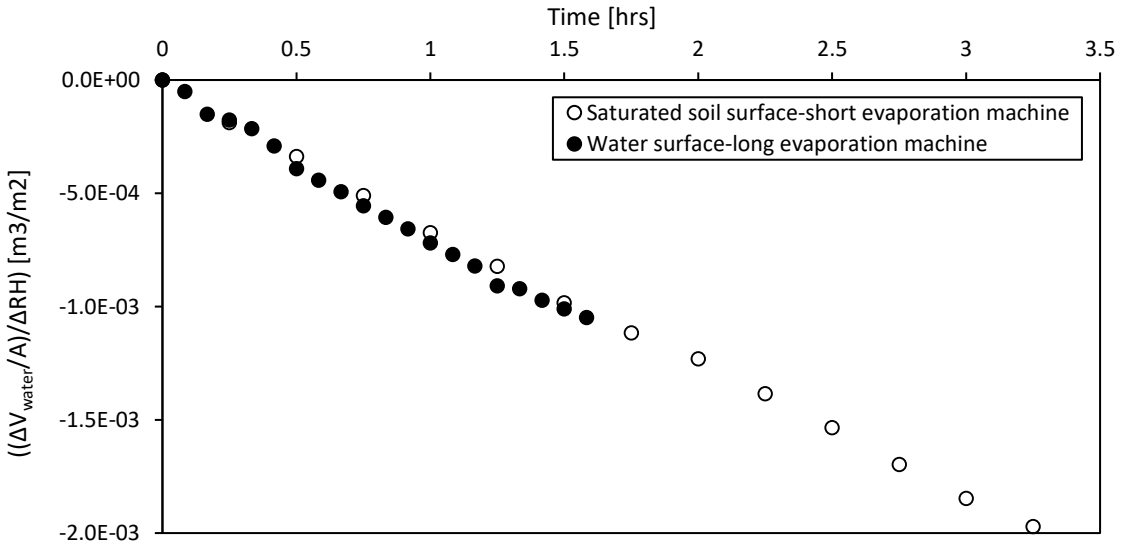

Figure 18: Evaporation rate of water from the saturated soil sample and from the water surface in tests with airflow at v_{air}=4m/s and RH_{inlet}=0%

6 Discussion

The key parameter of the model to simulate the evaporation rate is the vapour convection volume transfer coefficient α in equation (9). In Section 5.1, the coefficient α was calibrated for tangential airflow associated with Reynolds numbers in the range 2300-10000, which is in turn associated with the transition zone between laminar and turbulent regime. A critical point to address is whether the air flow and the evaporation thereof occurs under conditions closer to laminar or turbulent regime. For example, if evaporation in the experiments is associated with turbulent regime, any increase in the air gap would generate higher Reynolds numbers, airflow would definitely be turbulent, and the convection volume transfer coefficients derived experimentally would still hold. On the other hand, any decrease in the air gap will generate lower Reynolds number, airflow would tend to become laminar and a new evaporation machine with lower height of the wind tunnel should be implemented to investigate laminar conditions.

To investigate the airflow regime, the vapour convection volume transfer coefficients inferred experimentally from the wind tunnel tests (Table 4) under conditions of internal flow were compared with theoretical formulations available in the literature, even if the latter were derived for external flow conditions (open surface evaporation).

The dynamic surface sublayer of the atmospheric boundary layer is a fully turbulent region far enough from the evaporating surface where both viscosity of the air and the structure of the individual roughness elements of the surface have no effect on the motion. In this layer, the vertical profiles of air velocity and vapour concentration can be assumed to be logarithmic (Brutsaert, 1982). Under these assumptions, the convection volumetric transfer coefficient can be expressed as follows (see Appendix II):

$$\alpha = \frac{0.622}{\rho_w R_d T} \cdot \frac{k^2 \cdot v_{air}(z)}{ln^2\left(\frac{z - d_0}{z_{0m}}\right)} \tag{13}$$

where k is the Karman's constant, R_d is the gas constant of dry air, T is the absolute temperature at the reference height z from the wet surface, p_{vo} is the vapour pressure at saturation, $RH(z)$ is the relative humidity of the airflow at the reference height z from the wet surface, ρ_w is the density of liquid water, z_{0m} is the momentum roughness parameter, and d_0 is the zero-plane displacement height (Brutsaert, 1982).

Expressions for the convective volume transfer coefficient can also be derived for the case of external air flow parallel to evaporating surface. External flow occurs when the boundary layers develop freely without constraints imposed by adjacent surfaces and there exists a 'free stream' region of flow outside the boundary layer where velocity and concentration gradients are negligible. Under these assumptions, the convection volumetric transfer coefficient can be expressed as follows (see Appendix III):

$$\alpha = \frac{M_w}{\rho_w \cdot R \cdot T}\frac{D_{va}}{L}0.332\frac{1}{L}\int_{\xi}^{\xi+L}\frac{\left(\frac{v_{air}\cdot x}{\nu}\right)^{\frac{1}{2}}\left(\frac{\nu}{D_{va}}\right)^{1/3}}{\left[1-\left(\frac{\xi}{x}\right)^{3/4}\right]^{1/3}}dx \quad (laminar\ regime) \tag{14a}$$

$$\alpha = \frac{M_w}{\rho_w \cdot R \cdot T}\frac{D_{va}}{L}0.0296\frac{1}{L}\int_{\xi}^{\xi+L}\frac{\left(\frac{v_{air}\cdot x}{\nu}\right)^{4/5}\left(\frac{\nu}{D_{va}}\right)^{1/3}}{\left[1-\left(\frac{\xi}{x}\right)^{9/10}\right]^{1/9}}dx\ (turbulent\ regime) \tag{14b}$$

where R is the universal gas constant, M_w id the water molar mass, L is the length of the evaporating surface, D_{va} is the diffusion coefficient of vapour in air, v_{air} is the free stream air velocity, ν is the kinematic viscosity of air, x is the distance from the leading edge of the flat plate, and ξ is the non-evaporating starting length.

These equations are compared with the experimental data in Figure 19. It appears that the two equations derived under the assumption of turbulent regime (Equations (13) and (14b)), match fairly well the experimental data, even if these equations were obtained for external flow conditions. On the other hand, the equation derived for laminar regime (Equation (14a)) significantly underestimates the experimental data. This clearly suggests that evaporation occurred under turbulent conditions in the wind tunnel.

Finally, an equation for the convective volume transfer coefficient for evaporation form open surface can be derived from Penman (1948) as discussed in Appendix IV:

$$\alpha = \frac{0.622}{\rho_w R_d T} \cdot \frac{250}{0.5 + 0.54 \cdot v_{air}(z)} \alpha \tag{15}$$

and this also matches fairly well the experimental data.

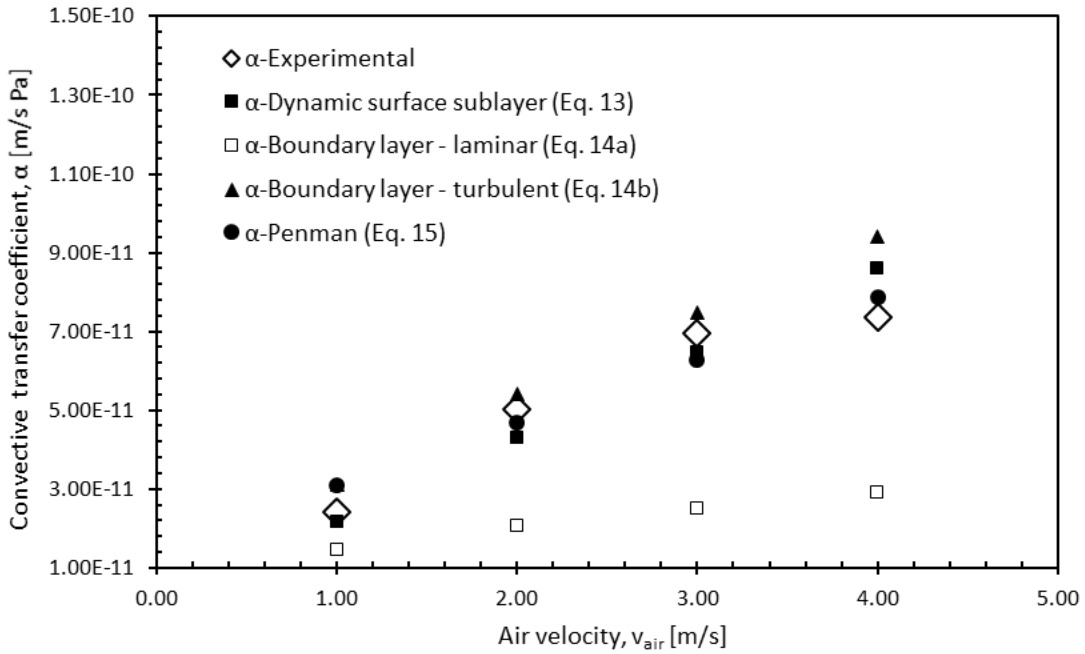

Figure 19: Comparison experimental and theoretical values of the convective vapour transfer coefficient α.

The very good prediction based on equations derived for 'open surface' evaporation obtained by replacing the free stream air velocity with the mean air velocity in the wind tunnel seems to suggest that the boundary layer in the wind tunnel remains relatively thin then corroborating the assumption made in Figure 16 about the distribution of air velocity and relative humidity across the wind tunnel section. Indeed, Brutsaert (1982) suggests that the interfacial sublayer is 1.5 to 3.5 times the height h_0 of the roughness obstacles. In the evaporation machine the surface exposed to evaporation is a smooth surface with virtually zero roughness. The interfacial sublayer is therefore expected to be very small so that the anemometer at 20mm from the evaporating surface measures air velocity in the fully developed logarithmic profile.

For the case of the suction drain in the field, soil surface roughness would be greater than the roughness of the free water in the wind tunnel. This would generate higher values of the parameter z_{0m} in Equation (13) and, hence, higher values if the convective volume transfer coefficient. As a result, the values derived experimentally for the case of a free water surface would lead to conservative prediction.

7 Conclusions

The paper has presented an experimental investigation of the evaporation from water and soil surfaces induced by tangential air flow through a confined space. This study was aimed at supporting the design of suction drains, a technique for low carbon temporary stabilisation of tunnels and excavations in clays.

An apparatus was developed to measure water evaporation from a 3m long wet surface subjected to a tangential airflow through a 40mm gap. Tests have explored different air velocities (1 to 4m/s) and relative humidity at the inlet (RH=0% and RH=30%). As expected, experimental results showed that i) evaporation rate increased with air velocity, ii) evaporation rate decreased with RH at the inlet of the airflow, and iii) relative humidity increased along the wet surface, i.e. the airflow progressively enriched with water vapour.

The relationship derived experimentally between the evaporation rate along a 3m wet surface and the air velocity and relative humidity of the airflow cannot be applied straightway to longer or shorter evaporation surfaces. For this reason, a simple evaporation model was developed based on the assumption that relative humidity and velocity of airflow are uniform in the confined space.

The key parameter of the model is the vapour transfer coefficient α, which controls the linear dependency of the evaporation rate on the relative humidity differential between the wet surface and the airflow. The vapour transfer coefficient α was calibrated against the tests with relative humidity at the inlet RH_{inlet}=0% and this allowed probing the model against the tests

with relative humidity at the inlet RH_{inlet}=30%. The model was found to perform satisfactorily showing that the simple assumption of uniform relative humidity and velocity does not represent a significant limitation of the model.

The vapour transfer coefficient α detected in the test on water surface was then found to be the same as the vapour transfer coefficient for saturated soil exposed to the airflow. As a result, findings from tests on water surfaces can be extrapolated to soil surfaces.

The values of vapour transfer coefficient derived theoretically for the case of external flow were then compared with the values obtained experimentally. The good matching with the values derived for turbulent regime suggests that evaporation in the wind tunnel occurred under this regime. In addition, the good performance of the open surface' equations suggest that the boundary layer remains relatively thin in the wind tunnel this corroborating the assumption about the profile of air velocity and relative humidity made to develop the simple evaporation model.

8 Acknowledgment

This work was supported by University of Strathclyde,

9 References

Barghi, M. H. (2018). *Use of capillary action to control soil moisture*. PhD dissertation, University of Birmingham

Brutsaert, W. (1982). *Evaporation into the atmosphere: theory, history and applications.* Springer Science & Business Media.

Chandavari, V., & Palekar, S. (2014). Diffuser angle control to avoid flow separation. *Int. J. Tech. Res. Appl, 2(5), 16-21*.

Chu, C. R., Li, M. H., Chen, Y. Y., & Kuo, Y. H. (2010). A wind tunnel experiment on the evaporation rate of Class A evaporation pan. *Journal of Hydrology, 381(3-4), 221-224.*

Comtebellot, G. (1976). Hot-Wire Anemometry. *Annual Review of Fluid Mechanics*, *8*(Thomas 1920), 209–231.

Davarzani, H., Smits, K., Tolene, R. & Illangasekare, T. (2014). Study of the effect of wind speed on evaporation from soil through integrated modeling of atmospheric boundary layer and shallow subsurface. *Water Resources Research*. 50. 11431-. 10.1002/2013WR013952.

de Métrologie Légale, O. I. (1996). The scale of relative humidity of air certified against saturated salt solutions. *International Recommendation, OIML*.

Garitte, B., Bond, A., Millard, A., Zhang, C., Mcdermott, C., Nakama, S. and Gens, A. (2013). Analysis of hydro-mechanical processes in a ventilated tunnel in an argillaceous rock on the basis of different modelling approaches. J*ournal of Rock Mechanics and Geotechnical Engineering*, 5. 1-17. DOI: 10.1016/j.jrmge.2012.09.001.

Greenspan, L. (1977). Humidity fixed points of binary saturated aqueous solutions. *Journal of Research of the National Bureau of Standards Section A: Physics and Chemistry*, *81*(1), 89–96.

Griffin, H & O'Kelly, B. (2014). Ground improvement by vacuum consolidation - a review. P*roceedings of the Institution of Civil Engineers, Ground Improvement.* 167. 274 - 290. 10.1680/grim.13.00012.

Incropera, F.P. and deWitt, D.P. (2002). *Fundamentals of Heat and Mass Transfer*. 3rd edn, pp. 385–466. John Wiley and Sons, USA.

Lim, W. H., Roderick, M. L., Hobbins, M. T., Wong, S. C., Groeneveld, P. J., Sun, F., & Farquhar, G. D. (2012). The aerodynamics of pan evaporation. *Agricultural and Forest Meteorology, 152, 31-43.*

Lozada, C., Caicedo, B. & Thorel, L. (2016). Improved climatic chamber for desiccation simulation. *E3S Web of Conferences*. 9. 13002. 10.1051/e3sconf/20160913002.

Lozada, C., Caicedo, B. & Thorel, L. (2018). A new climatic chamber for studying soil - atmosphere interaction in physical models. *International Journal of Physical Modelling in Geotechnics*. 1-31. 10.1680/jphmg.17.00073.

Martini, M., Tarantino, A. and Sloan, A. (2019. Suction drain as a low carbon ground improvement technique: proof-of-concept at the laboratory scale. Compoanion paper submitted to Tunnelling and Underground Space Technology.

Omega Engineering. (2018). User's Guide FMA1000 SERIES.

Penman, H. L. (1948). Natural evaporation from open water, bare soil and grass. *Proc. R. Soc. Lond. A, 193(1032), 120-145*.

Penman, H. L. (1956). Estimating Evaporation. *Eos, Transactions American Geophysical Union, 37(1), 43-50*.

Sakleshpur, V. A., Prezzi, M. & Salgado, R. (2018). Ground Engineering using Prefabricated Vertical Drains: A Review. *Geotechnical Engineering*. 49. 45-64.

Simpson, L. (2017). *Experimental Study of Induced Evaporation via the Suction Drain in Clayey Soils to Provide Tunnel Face Stability*. University of Strathclyde.

Song, W., Cui, Y-J., Tang, A-M, & Ding, W-Q (2013). Development of a Large-Scale Environmental Chamber for Investigating Soil Water Evaporation. *Geotechnical Testing Journal*. 36. 20120142. 10.1520/GTJ20120142.

Song, W., Cui, Y-J., Tang, A-M, Ding, W-Q & Tran, T. (2014). Experimental study on water evaporation from sand using environmental chamber. *Canadian Geotechnical Journal*. 51. 10.1139/cgj-2013-0155.

Tarantino, A. 2010. Basic concepts in the mechanics and hydraulics of unsaturated geomaterials. New Trends in the Mechanics of Unsaturated Geomaterials Lyesse Laloui (ed.), 3-28. ISTE – John Wiley & Sons.

Tarantino, A., Sacchet, A., Dal Maschio, R. & Francescon, F. (2010). A Hydromechanical Approach to Model Shrinkage of Air-Dried Green Bodies. *Journal of the American Ceramic Society, 93, No. 3, 662–670.*

Trombetti, F. and Tagliazucca, M. (1994). *Characteristic scales of atmospheric surface layer*. Technical Paper No. 4. FISBAT-TP-94/1. Istituto FISBAT-CNR, Bologna.

Talev, G., Gustavsen, A. & Næss, E. (2008). Influence of the Velocity, Local Position, and Relative Humidity of Moist Air on the Convective Mass Transfer Coefficient in a Rectangular Tunnel — Theory and Experiments. *Journal of Building Physics*, 32, 155-173. DOI: 10.1177/1744259108091564.

Thom, A. S., & Oliver, H. R. (1977). On Penman's equation for estimating regional evaporation. *Quarterly Journal of the Royal Meteorological Society, 103(436), 345-357*.

Winston, P. W., & Bates, D. H. (1960). Saturated Solutions For the Control of Humidity in Biological Research. *Ecology, 41(1), 232-237*.

Wood, D.M. (1991). Soil Behaviour and Critical State Soil Mechanics. Cambridge University Press

APPENDIX I – Measurement devices

Relative Humidity/Temperature (RH/T) sensors

The RH/T sensors installed in the long evaporation machine are Sensirion Kit EK-H5 capacitive sensors SHT21 with RH accuracy of ±2% (20%-80% RH) and ±3% (0-20% RH – 80%-100% RH) and temperature accuracy of ±0.3°C. The sensor size is 3 x 3 x 1.1 mm^3.

The relative humidity sensors were calibrated using the fixed-point humidity systems (de Métrologie Légale, 1996) with relative humidity fixed points (HFP) imposed via six saturated salt solutions and dry silica gel. The saturated salt solutions are listed in Table 5 together with the associated values of relative humidity and their uncertainty (3 times the standard deviation) according to (Greenspan, 1977). The aqueous saturated solutions were prepared according to (de Métrologie Légale, 1996). Demineralised water with electrical conductivity lower than 5.5 μS/m was used to prepare the aqueous saturated solutions. The amount of salt mixed with the demineralised water was about twice the value corresponding to the saturated conditions to ensure that precipitated salt remained clearly visible.

The aqueous solutions were prepared in six separated containers 48 hours prior to the RH measurement to allow the thermodynamic equilibrium between the solid (salt precipitation) the liquid (solution). The containers were filled with the same amount of aqueous solution to leave a headspace between the water level and the rim of the container equal to 30 mm. Each container was closed with an air-tight lid and placed in water bath in a temperature-controlled room (20±0.5°C). An additional container was filled with silica gel to leave the same headspace and placed in the same water bath.

Table 5: Standard relative humidity value for saturated salt solution at 20°C

Salt solution	Standard relative humidity (%)	Uncertainty (%)
$MgCl_2$	33.07	±0.18

K_2CO_3	43.16	±0.33
KI	69.90	±0.26
NaCl	75.47	±0.14
KCl	85.11	±0.29
$CuSO_4$	98.00	N/A

Source: All values from (Greenspan, 1977) except $CuSO_4$ from (Winston & Bates, 1960)

The electrical parts of the RH/T sensors were spray-coated with Servisol Plastic Seal 60 Protective Insulator to protect from oxidation. Parafilm® was used to cover the connection between the sensor and the electrical cable. A single extra lid was drilled with six small holes and the sensor cables were passed through them. The cables were sealed with silicone and the sensors were connected to the cables on the inner side of the lid. The sensors were all hanging from the lid at the same height in the container headspace.

The lid carrying the six RH/T sensors was placed onto the container with the lower relative humidity fixed point (silica gel). The sensors remained in each container for 24h, a time sufficient for the sensor readings to stabilise. The lid was then removed and placed on the following container. The RH was increased from 0% to 98% and then decreased to 0%.

The calibration curve was derived by establishing a correlation between the relative humidity RH imposed and the sensor output. The sensor output consisted in a nominal RH based on manufacturer calibration. The calibration curve is linear in the range 0-70% with negligible hysteresis (Figure 20). The calibration curve was derived in this range only, which encompasses the values measured in the tests in this experimental programme.

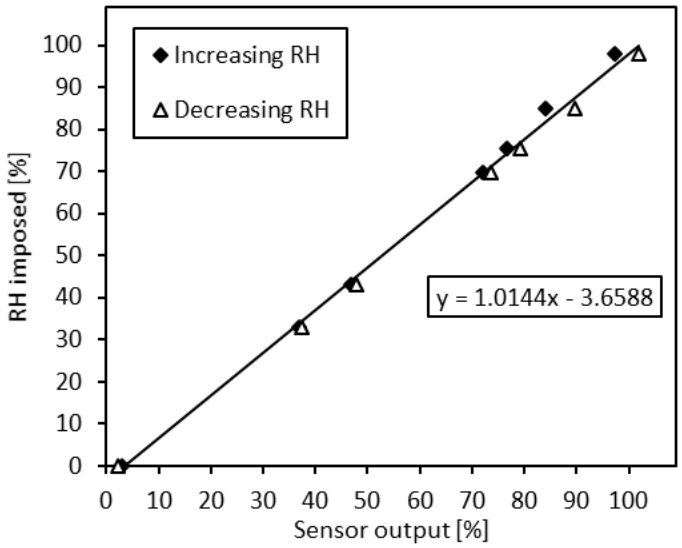

Figure 20: Typical calibration curve of the RH/T sensor

The RH/T sensors were not calibrated with respect to temperature. However, the temperature returned by the sensors based on manufacturer calibration was checked by comparison with a high-precision reference temperature sensors (Fluke 5641-P Thermistor Probe). The RH/T sensors were wrapped together with the high precision reference temperature sensors in foam sheet and discrepancies were found to be lower than ±0.2°C. This accuracy was considered acceptable for the purpose of this study.

Anemometer

The anemometer used in both the short and the long evaporation machine to monitor the airflow velocity was OMEGA FMA1006R-V2-S. The sensor design is based on three RTD elements, one measures the air temperature and the other two measure the air velocity. The air velocity is measured based on the heat loss from the RTD velocity sensor as it cools down by the air flow (Omega Engineering, 2018).

To assess the accuracy of the anemometer measurements, the anemometer was installed in a wind-tunnel normal to the airflow and firmly connected to a support to prevent vibration at high velocity. Air velocity was increased from 3m/s to 8m/s in steps then decreased to 3m/s. The air velocity measured by the anemometer was benchmarked against a Pitot tube. For each

step, the measurement of air velocity from both anemometer and Pitot tube was taken once the air velocity stabilised (typically in less than 2 min). At relatively low air velocity (<2-3m/s), Pitot tubes are not sensitive enough (Comtebellot, 1976), thus 3m/s was the lowest air velocity imposed in the wind-tunnel. The tests were carried out at a temperature of 20°C ± 0.5°C.

The measurements by the anemometer are compared with the measurement by the Pitot tube in Figure 21. There was no apparent hysteresis and the standard deviation of the error was less than 0.13 m/s. The response of the anemometer in the range was taken as an evidence of satisfactory performance of the anemometer. It was therefore assumed the measurements were accurate also in the range 0-3m/s.

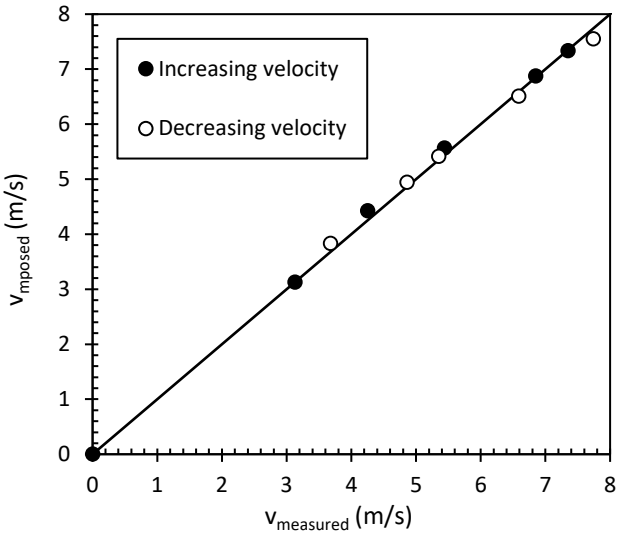

Figure 21: Calibration curve of the anemometer

Balances

The balances used in the long evaporation were ADAM CBK-32 and ADAM CBK-48 with the maximum capacity equals to 32kg and 48kg and accuracy according to manufacturer's specifications equal to 1g and 2g, respectively. The balance used in the small evaporation machine was ADAM PGW6002e with the maximum capacity equals to 6kg and the accuracy according to manufacturer's specifications equal to 0.1g. To assess the accuracy of the balance measurements, a weight equal to 11110g was placed on the balances used in the long evaporation machine to mimic the weight of half of the long evaporation machine. Similarly,

a weight equals to 6110 g was placed on the balance used in the short evaporation machine to mimic the weight of the short evaporation machine. Weights were added to the balances in the from 1g to 5000 g in the sequence 1/2/5 and then removed by inverting the sequence to mimic the variation of water mass occurring in the evaporation machines. The standard deviation of the error was found to be less than 1.3 g for the balances used for the long evaporation machine and less than 0.3 g for the balance used for the short evaporation machine.

APPENDIX II – Convective volume transfer coefficient in fully turbulent dynamic surface sublayer

The dynamic surface sublayer of the atmospheric boundary layer is a fully turbulent region far enough from the evaporating surface that both viscosity of the air and the structure of the individual roughness elements of the surface have no effect on the motion. In this layer, the vertical profiles of air velocity and vapour concentration are logarithmic (Brutsaert, 1982).

Under these conditions, the water vapour flux at the surface q can be written as follows:

$$q = \underbrace{\left[\frac{0.622}{\rho_w R_d T(z)} \cdot \frac{k^2 \cdot v_{air}(z)}{ln^2\left(\frac{z-d_0}{z_{0m}}\right)}\right]}_{\alpha} \cdot p_{v0}\,(1 - RH(z)) \tag{16}$$

where k is the Karman's constant (k=0.41) R_d is the gas constant of dry air ($R_d = 287.04\ J\ K^{-1}\ kg^{-1}$), *T(z)* is the absolute temperature at the reference height z from the wet surface, p_{vo} is the equilibrium vapour pressure at saturation, $RH(z)$ is the relative humidity of the airflow at the reference height z from the wet surface, ρ_w is the density of liquid water, z_{0m} is an integration constant whose dimensions are length and is referred to as momentum roughness parameter, and d_0 is the zero-plane displacement height that is different from zero for the case of rough surfaces (Brutsaert, 1982). The parameter can be visualised graphically as the zero velocity intercept of the logarithmic velocity profile (Figure 22). The term in the square bracket in Eq. (16) represents the convective volume transfer coefficient. For the wind channel in tested in this experimental programme, it was assumed z=20mm, d0=0, and z_{0m}=0.00001m according to Trombetti and Tagliazucca (1994) for smooth surfaces.

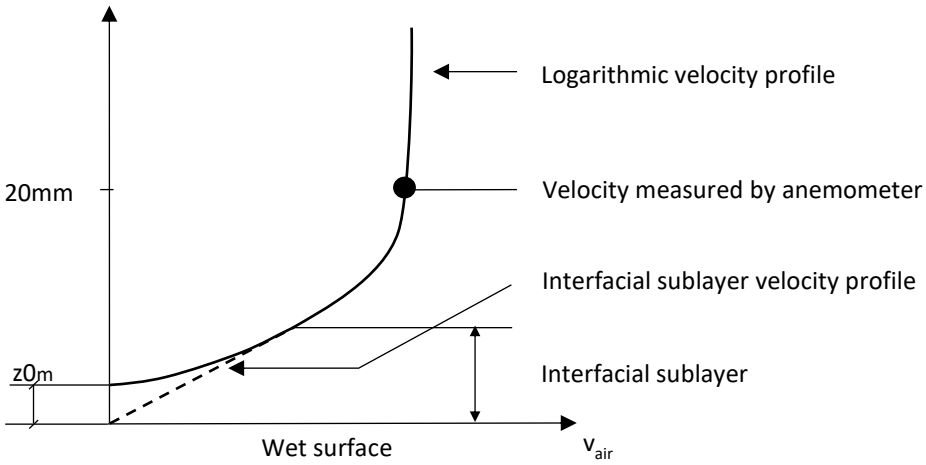

Figure 22: Air velocity logarithmic profile in the dynamic sublayer

APPENDIX III – Convective volume transfer coefficient for parallel external flow

Expressions for the convective volume transfer coefficient can be derived for the case of external air flow parallel to evaporating surface. External flow occurs when the boundary layers develop freely without constraints imposed by adjacent surfaces and there exists a 'free stream' region of flow outside the boundary layer where velocity and concentration gradients are negligible. Water vapour flux q can be expressed as follows (after Incropera and deWitt, 2002).

$$q = \underbrace{\left[\frac{M_w}{\rho_w \cdot R \cdot T} h_m\right]}_{\alpha} \cdot p_{v0}\,(1 - RH_\infty) \tag{17}$$

where T is the absolute temperature assumed to be the same for the evaporating surface and the free stream, R is the universal gas constant, ρ_w is the water density, M_w id the water molar mass, weight, p_{vo} is the equilibrium vapour pressure at saturation, RH_∞ is the free stream relative humidity, and h_m [m/s] is the convection mass transfer coefficient . As a result, the local convection volume transfer coefficient is given by:

$$\alpha = \frac{M_w}{\rho_w \cdot R \cdot T} h_m \tag{18}$$

The convection mass transfer coefficient h_m can be derived from the local Sherwood number as follows (Incropera and deWitt, 2002):

$$h_m = \frac{D_{va}}{L} Sh \tag{19}$$

where L is the length of the evaporating surface and D_{va} is the diffusion coefficient of vapour in air. In turn, the local Sherwood number is given by (Incropera and deWitt, 2002):

$$Sh = \frac{0.332 \cdot \left(\frac{u_\infty \cdot x}{\nu}\right)^{\frac{1}{2}} \left(\frac{\nu}{D_{va}}\right)^{1/3}}{\left[1 - \left(\frac{\xi}{x}\right)^{3/4}\right]^{1/3}} \qquad (laminar\ regime) \tag{20}$$

$$Sh = \frac{0.0296 \cdot \left(\frac{u_\infty \cdot x}{\nu}\right)^{4/5} \left(\frac{\nu}{D_{va}}\right)^{1/3}}{\left[1 - \left(\frac{\xi}{x}\right)^{9/10}\right]^{1/9}} \qquad (turbulent\ regime)$$

where u_∞ is the free stream air velocity, ν is the kinematic viscosity of air, x is the distance from the leading edge of the flat plate, and ξ is the non-evaporating starting length (Figure 23). By combining Equations (18), (19), and (20), the local convective volume transfer coefficient α can be derived as a function of the distance x from the leading edge of the flat plate. In this exercise, an average convective volume transfer coefficient between ξ and L was considered (with ξ=0.5m and L=3 m as shown in Figure 2)

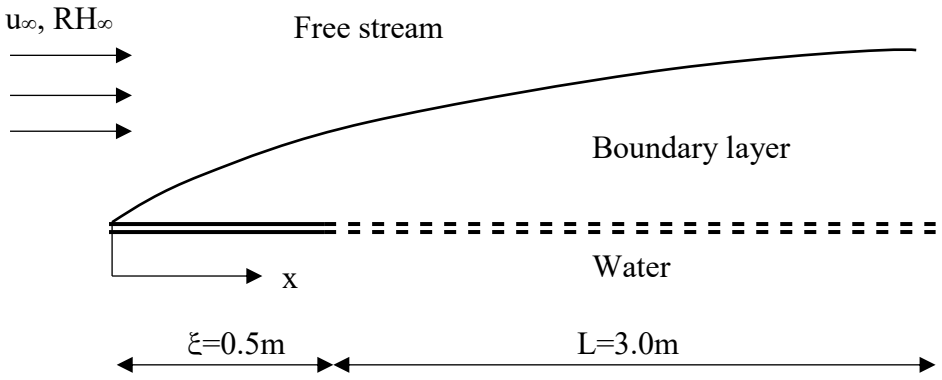

Figure 23: Flat plate in parallel flow with impermeable starting length

APPENDIX IV – Penman's convective volume transfer coefficient

Penman (1948) provides a theoretical equation for the estimation of the evaporation rate q from open water surface by using the standard meteorological data at the reference height z=2m from the wet surface. According to Brutsaert (1982), this can be expressed as:

$$q = \frac{0.622}{\rho_w R_d T(z)\, r_a} \cdot p_{v0}\,(1 - RH(z)) \tag{21}$$

where 0.622=(18.016/28.966) is the ratio of the molecular weights of water and dry air, ρ_w is the density of water, R_d is the gas constant of dry air ($R_d = 287.04\, J\, K^{-1}\, kg^{-1}$), *T(z)* is the absolute temperature at the reference height z from the wet surface, p_{vo} is the equilibrium vapour pressure at saturation, $RH(z)$ is the relative humidity of the airflow at the reference height z from the wet surface, and r_a is the aerodynamic resistance. The latter was expressed by Penman, (1956) as follows (Brutsaert, 1982, Thom & Oliver, 1977):

$$r_a = \frac{250}{0.5 + 0.54 \cdot v_{air}(z)} \quad \left[\frac{s}{m}\right] \tag{22}$$

where $v_{air}(z)$ is the air velocity measured at reference height from the wet surface.

By combining equation (21) and (22), the evaporation rate E (m/s) (volume of water per unit time and unit area) can be calculated as follows according to Penman:

$$q = \underbrace{\left[\frac{0.622}{\rho_w R_d T(z)} \cdot \frac{250}{0.5 + 0.54 \cdot v_{air}(z)}\right]}_{\alpha} \cdot\ p_{v0}\,(1 - RH(z)) \tag{23}$$

with the term in square bracket representing the convective volume transfer coefficient.

It is worth noticing that equation (23) also applies to soils under both saturated and unsaturated conditions provided the relative humidity at evaporating surface, which is equal to 1 for the case of free water, is replaced by the relative humidity at the soil surface given by the psychometric law as discussed in Martini et al. (2019).

For the case of the wind tunnel tested in the experiments presented in the paper, the relative humidity and the air velocity were calculated at z=20mm above the wet surface in place of the reference height of z=2m as per the original Penman's equation.